UNIVERSITY OF CALIFORNIA

SANTA CRUZ

Environmental Changes on the North American Mid-Atlantic Shelf During the Paleocene Eocene Thermal Maximum

A thesis submitted in partial satisfaction
of the requirements for the degree of

MASTER OF SCIENCE

in

EARTH SCIENCES

By

Edward A. Ballaron

September 2018

The Thesis of Edward A. Ballaron is approved:

Dr. James Zachos

Dr. Mathew Clapham

Dr. Terry Blackburn

Lori Kletzer
Dean of Graduate Studies

Table of Contents

Abstract

Environmental Changes on the North American Mid-Atlantic Shelf During the Paleocene Eocene Thermal Maximum

Edward A. Ballaron

The Paleocene-Eocene Thermal Maximum (PETM), a large hyperthermal during the Cenozoic (~56 Ma) is characterized by a massive injection of depleted carbon into global reservoirs as indicated by a large negative carbon isotope excursion (CIE) of 3‰-5‰ in marine and terrestrial sedimentary records. Previously studied open ocean (i.e., pelagic) cores have provided evidence for abrupt sea surface warming (5-10°C) and bottom water warming (4-5°C) as well as ocean acidification at the onset of the CIE. However, due to low sedimentation rates and truncation of pelagic sections via dissolution at the CIE, pelagic cores appear condensed or incomplete. Sites on the North American mid-Atlantic margin, provide a unique opportunity to examine both marine and terrestrial responses to a large magnitude climatic perturbation. Rapid and abrupt increases in the flux of siliciclastics including kaolinite to the shelf at the onset of the PETM, indicative of an enhanced hydrologic cycle, result in expanded PETM intervals allowing for higher resolution isotopic sampling. Stable isotopic and trace metal data from New Jersey sections (Millville, Ancora, Bass River and Wilson Lake) have also documented rapid warming, coastal ocean

acidification and a freshening event at the onset of the CIE in agreement with evidence for an enhanced hydrologic cycle during the PETM. Maryland sections to the south (South Dover Bridge and Cambridge-Dorchester) studied here, are more proximal to the main drainage system in the Salisbury Embayment and therefore should have experienced environmental changes (salinity) to a greater degree than New Jersey sites. Here we present coupled stable isotopic (carbon and oxygen) and trace metal data (Mg/Ca) to constrain both changes in temperature as well as salinity on the Maryland mid-Atlantic shelf during the PETM. Data presented here shows a temperature increase at SDB and Cam-Dor of ~4-5°C for planktonic foraminifera and ~5-9°C for benthic foraminifera with oxygen derived temperatures being consistently larger than Mg/Ca derived temperatures. This indicates some salinity contribution to $\delta^{18}O$, artificially lowering oxygen derived temperatures. This is further supported by salinity calculations which display a freshening event at the onset of the CIE due to increased runoff. Also observed in this data set is a slight weakening in $\delta^{13}C$ and $\delta^{18}O$ depth gradients on the shelf. Changes in $\delta^{18}O$ gradients can perhaps be attributed to greater warming at depth and a destabilization of the thermal stratification of the water column, similar to observations from New Jersey sites Millivlle and Ancora. The breakdown in vertical $\delta^{13}C$ gradients was perhaps due to the vertical migration of mixed layer foraminifera taxa seeking refuge from warming surface waters. Another possible explanation for the change in

vertical $\delta^{13}C$ gradients is a change in upwelling patterns driven by hyperpycnal flow or changes in wind patterns driving coastal upwelling and bringing depleted $\delta^{13}C$ to the surface.

Acknowledgements

I would first like to acknowledge Dr. James Zachos for being a kind, knowledgeable and always available advisor. As an undergrad, I was given the opportunity to work in the lab where I gained valuable experience crucial to the field of Paleoclimatology. His belief in me allowed me to gain acceptance into the Master's program at UCSC and his guidance made the research process smooth and enjoyable.

Dr. Tali Babila also played an important role in this project by sharing unpublished data. Her knowledge of shelf processes and previous work done in New Jersey and Maryland provided a template for my research. Her knowledge of ICP-MS was also necessary for completion of this project.

Special thanks go to Dr. Marci Robinson and Dr. Jean Self-Trail at the USGS as well as Dr. Peter Stassen for guidance with research done on the mid-Atlantic shelf and help identifying the appropriate foraminifera genera.

My thanks also go to Dustin Harper and William Rush for advice, instrumentation guidance and help with the salinity calculation process. Further thanks go to undergrads Cheyne Hirota and Demir Worthington for assistance conducting isotopic analyses and sample processing.

Additionally, I would like to acknowledge Dr. Matthew Clapham as well as Dr. Terry Blackburn for agreeing to be on my graduate committee and for

their valuable input and edits.

I would also like to acknowledge NSF for funding my research and allowing me the opportunity to contribute knowledge to the scientific community. Thank you to the faculty and fellow graduate students of the Earth and Planetary Sciences department at UC Santa Cruz for their instruction and support.

Finally, I would like to thank my father Steve Ballaron for instilling in me an interest in science and my mother Silveria Arrizón Ballarón for reminding me that creativity is also an important part of the scientific process. Gracias por todo.

I. INTRODUCTION

The most prominent hyperthermal event of the Cenozoic, the Paleocene-Eocene Thermal Maximum (PETM), has drastically changed our understanding of how changes in global carbon reservoirs can have long lasting environmental effects. The PETM, ~56 Ma, is characterized by a rapid and large negative carbon isotope excursion (CIE) of 3‰-5‰ in terrestrial and marine records (e.g., Kennett and Stott, 1991; Koch et al., 1992; McInerney and Wing, 2011). As evidenced by ocean acidification (Zachos et al., 2005; Penman et al, 2014), the CIE reflects a massive injection of depleted carbon into global reservoirs and a subsequent increase in global sea surface and bottom-water temperatures of 8-10°C and 4-5°C respectively (Kennett and Stott 1991; Zachos et al., 2003). Several mechanisms have been implicated as the source of carbon initiating this climatic perturbation, including methane clathrates, injection of magma into organic rich sediments, comet impact, wildfires and carbon release from thawing permafrost (McInerney & Wing, 2011). Whatever the source, the addition of CO_2 into the atmosphere would have had serious impacts on marine and terrestrial climates and environments.

Most past studies of the climatic changes associated with the PETM have focused on the open ocean (e.g. pelagic cores) or continental interiors. In contrast, continental shelf environments have been understudied, leading

to an overall lack of knowledge of the climatic and environmental impacts of the PETM on coastal regions. This is a serious deficiency as coastal oceans should be highly sensitive to the impacts of global warming and associated changes in the hydrologic cycle. One region where this deficiency is being rectified is along the New Jersey and Maryland coastal plain in the Salisbury Embayment (Figure 1). Several sedimentary sections are of special significance in this region due to accelerated sedimentation rates and increased clay content, which yield expanded sections of the CIE onset and recovery (Gibson et al., 2000). Moreover, because of the proximity to major drainages, these sections are ideally located to capture important climatic, biogeochemical and ecosystem responses such as an intensification of the hydrologic cycle, acidification, and eutrophication.

The first detailed multiproxy studies of shallow marine environments during the PETM were completed on land-based sections in New Jersey: Bass River, Wilson Lake, Clayton, Ancora and Millville (Zachos et al., 2006; Stassen et al., 2012; Babila et al., 2016; Makarova et al., 2017). The basal upper Paleocene unit of these sections is represented by the Vincentown Fm., which is predominantly comprised of abundant quartz and glauconite. This is typically overlain by the Marlboro Fm., representing the core of the CIE and recovery, characterized by fine/silty sand and clay, generally associated with transgression and deeper water (Sluijs et al., 2009). This transition is marked by a dissolution zone where $CaCO_3$% decreases markedly within the

onset of the CIE. This is followed by the Manasquan Fm. which unconformably overlies the Marlboro Fm. (Stassen et al., 2012). The unconformity is associated with a sea level regression which tends to truncate the Marlboro Clay to varying extents generally depending on site proximity to the coast line.

Sections in Maryland (South Dover Bridge, Cambridge-Dorchester and Mattawoman Creek-Billingsley Road) to the southwest (Figure 1) display a similar lithologic sequence as the New Jersey Sites, though with some minor differences. The basal unit at these sites is represented by the latest Paleocene Aquia Fm. comprised of glauconitic-quartz rich sand. This is overlain by the basal Eocene micaceous clay unit Marlboro Clay (12 to 15 m thick). Unconformably overlying the Marlboro Clay is the early Eocene Nanjemoy Fm. composed of silty to sandy clay (Self-Trail et al., 2012) (Figure 2).

The marine paleotemperature reconstructions for the New Jersey margin based on oxygen isotopes and TEX_{86} indicate SST warming of 5 to 8°C during the CIE (Zachos et al., 2006; John et al., 2008). These estimates have been more or less supported by Mg/Ca based estimates of SST (Babila et al., 2016). However, given the evidence of an enhanced hydrologic cycle and resulting increased runoff (in response to warming) it's possible the $\delta^{18}O$ temperature estimates are biased upward by a local decline in seawater $\delta^{18}O$

(i.e., salinity) associated with enhanced precipitation/runoff, though it's not obvious whether the planktonic foraminifera would have been present during periods of excessive freshening of the coastal ocean.

The evidence for an enhanced hydrologic cycle and runoff is diverse and includes a marked transition in the % kaolinite (relative to other clays) along with a rapid increase in siliciclastic accumulation rates over the CIE within the Marlboro clay (Gibson et al., 2000; Stassen et al., 2012). Moreover, evidence for uncharacteristically depleted dissolved oxygen levels are also attributed to seasonally increased freshwater input, stratification and local eutrophication (Lippert and Zachos, 2008; Self-Trail et al., 2017).

To extend our understanding of the mid-Atlantic coastal response beyond the NJ margin, this study focuses on sections in Maryland. This is particularly crucial given that the major drainages of the Appalachians and coastal plain were to the south of NJ in the vicinity of the modern Chesapeake Bay. In theory, we would expect a fairly exaggerated runoff response if the intensity of precipitation increased during the PETM all along the mid-Atlantic coastal region. Such an event should be manifested in a decline in sea surface salinity (SSS) that should be captured by foraminifera $\delta^{18}O$, for example, toward lower values if mean annual precipitation increased regionally as indicated by the NJ records. In addition to the changes in salinity, other spatial patterns related to latitude should be apparent, for

example a north to south thermal gradient.

Here we present new paleoceanographic records from mid-Atlantic sites South Dover Bridge (SDB) and Cambridge-Dorchester (Cam-Dor) based primarily on geochemical analyses of planktonic foraminifera genera *Morozovella* spp*., Acarinina* spp., and *Subbotina* spp*.* as well as benthic foraminifera *Cibicidiodes* spp*.* and *Anomalinoidies acutus*. Carbon, oxygen and trace metal (Mg/Ca) data were measured on all specimens in order to constrain both timing and distribution of climatic fluctuations along the North American continental margin during the PETM. This includes assessing changes in spatial and vertical temperature and salinity gradients on the shelf.

II. MATERIAL AND METHODS

2.1 Sample Processing

The South Dover Bridge (SDB) and Cambridge-Dorchester (Cam-Dor) sections are both comprised of sediments of the Paleocene Aquia Fm. overlain by the early Eocene Marlboro Clay and Nanjemoy Fm. (Self-Trail et al. 2012). The primary facies indicate deposition in inner to outer continental self-settings at water depths ranging from 50-150 m (Stassen et al., 2015; Self-Trail et al., 2017). The sampled PETM interval ranges from depths of 182.9 to 210 m and 204.4 to 230.1 m respectively. Sediment samples were taken at varying resolutions (0.3 to 2 m) from cores stored at the United States Geologic Survey, Reston, VA, and then processed at UC Santa Cruz.

Samples processed at UCSC were freeze dried and soaked in sodium hexametaphosphate Calgon solution $(NaPO_3)_6$ and left to disaggregate. Next, the sediments were washed through a 63μm sieve and dried. Each sample was then sieved into 180-212μm, 212-250μm, 250-300μm and 300-355μm size fractions and picked for planktonic foraminifera genera *Morozovella* spp*., Acarinina* spp., and *Subbotina* spp*.* as well as benthic foraminifera *Cibicidoides* spp*.* and *Anomalinoidies acutus.* The *Morozovella* spp. and *Acarinina* spp. genera are dominated by species of mixed-layer taxa that likely hosted photosymbionts whereas *Subbotina* spp*.* were thermocline dwellers (D'Hondt et al., 1994; Pearson et al., 2006). Due too low abundances of specimens, some foraminifera were sampled and analyzed at the genus level. Because the latest Paleocene Aquia Fm. is dominated by assemblages of epifaunal benthic foraminifera *Cibicidoides* spp. whereas the early Eocene Marlboro Clay is dominated by *A. acutus*, we must use both taxa in our P-E temperature reconstructions. While differences in vital effects between these two genera may introduce some error in the temperature calibrations, their similar habitats, life cycles and physiology makes this not likely. Additionally, given the large magnitude of isotopic changes across the CIE during the PETM, any error introduced is most likely negligible.

2.2 %$CaCO_3$ and Stable Isotopes

Bulk sediment was first freeze-dried and then pulverized using a mortar and pestle. For % $CaCO_3$ analysis, 20 mg of material from each

sample was weighed on a microbalance and placed in test tubes for work on the coulombmeter. In this system samples were dissolved in 2 N sulfuric acid (H_2SO_4) which generates CO_2 which is quantified via titration.

For stable C and O isotope analysis, 2-5 foraminifer shells were weighed by microbalance with sample masses typically falling between 15 to 30 µg. Shells were then roasted in an oven at 380°C to remove organic matter. Samples were analyzed by the Kiel /Mat253 gas source mass spectrometer system housed in the Stable Isotope Lab (SIL) at UCSC. Each sample run (n=30) included 10 standards of CM12, NBS18 and Atlantis II. In the Kiel Carbonate system, samples are dissolved in individual vessels with several drops of phosphoric acid (H_3PO_4) and the resulting CO_2 is distilled in a single step. The $\delta^{13}C$ and $\delta^{18}O$ values are reported in the delta notation where:

$$\delta(‰) = \left[\left(\frac{R_{sample}}{R_{standard}}\right) - 1\right] * 1000$$

and are relative to vPDB and carry an analytical error of ±0.05‰ and ±0.08‰ for $\delta^{13}C$ and $\delta^{18}O$ respectively based on repeated analyses of the CM12 standard (n=33).

2.3 Trace Metals

For analyses of major and minor trace elemental ratios (Mg, Sr, B), 40-60 foraminifera tests were picked from the 180-250 µm size fractions and cleaned using a multistep oxidative and reductive cleaning process (Barker et

al., 2003). Each sample of 40-60 specimens weighed between 200 and 400 µg. Foraminifera tests were then crushed between two glass slides to expose the inner test walls and placed inside vials, rinsed with a small amount of ddH_2O and alternated between an ultrasonic cleaner for 1-2 minutes and a hot water bath at 80 ºC for 5 minutes (3x). This same process was repeated using methanol (CH_4O) (2x) and a final rinse with ddH_2O. Next, to remove any metal oxides, samples are soaked in a solution of anhydrous hydrazine (NH_2NH_2), ammonium hydroxide (NH_4OH) and citric acid/ammonia solution ($C_6H_8O_7$)/(NH_3) for 30 minutes in a hot water bath while placing the vials in the ultrasonic cleaner every 2 minutes to prevent the oxides from re-precipitating. The samples are then rinsed with ddH_2O (3x). To remove organic matter, samples are soaked in a solution of hydrogen peroxide (H_2O_2) and sodium hydroxide (NaOH) at 80 ºC in a sonicator for 5 minutes. Samples were transferred to clean vials using Boron-free ddH_2O and a weak acid leach was performed using 0.001N nitric acid (HNO_3). Elemental analyses were conducted on a Thermo Finnigan Scientific Element XR Sector Field Inductively Coupled Plasma Mass Spectrometer (SF-ICP-MS) housed in the UCSC Marine Analytical Lab

III. RESULTS

3.1 Stable Isotopes- SDB

Bulk records generated by Self-Trail et al., (2012) show large

decreases across the Paleocene-Eocene boundary (i.e, Aquia to Marlboro Fm.). Within the upper portion of the Aquia the bulk $\delta^{13}C$ record shows an initial depletion of 2‰ at 207.3 m just below a larger excursion at 204.2 m. This initial negative excursion has been termed the pre-onset excursion (POE) which was first documented at a location outside the Salisbury Embayment (Bowen et al. 2014). Values recover back to baseline, followed by the primary onset of the CIE at 204.2 m depth with $\delta^{13}C$ values declining by 4‰ coincident with the transition from the Aquia to Marlboro Clay formation. Values slowly recover through the top of the Marlboro clay (~188 m), or at the transition to the Nanjemoy where the recovery appears truncated with carbon values shifting to a new baseline of 0.0‰, slightly lower than the pre-CIE baseline (Figure 2B). This pattern of a ~4‰ negative CIE and gradual but truncated recovery has been documented at other sites in the Salisbury Embayment including Bass River and Wilson Lake (Figure 3) (Zachos et al, 2006; John et al. 2008).

Planktonic foraminifera $\delta^{13}C$ values mirror the bulk record though consistently offset toward heavier values (Figure 2B). Through the POE interval, there is a 2‰ depletion in thermocline genera *Subbotina* spp. as well as in surface dwelling *Morozovella* spp. Pre-CIE carbon values for foraminifera calcite show $\delta^{13}C$ values in accordance with expected marine vertical gradients with surface dwelling genera *Acarinina* spp. and *Morozovella* spp. being slightly enriched relative to the thermocline dwelling

Subbotina spp. (D'Hondt et al., 1994). The CIE is marked by a 3-4‰ depletion in all planktonic foraminifera genera (Figures 2B) with a smaller decline recorded in thermocline dwelling genera. As a consequence, prior to the CIE, surface and mixed layer genera where separated by approximately 2.64‰ whereas post CIE values only show a separation of around 1.69‰. This mixed-layer to thermocline gradient on the shelf appears to re-stabilize as $\delta^{13}C$ values of surface and thermocline dwelling genera diverge to normal, however slightly depleted values.

Planktonic foraminifera $\delta^{18}O$ values show similar patterns to carbon trends, although there is no depletion at the POE in $\delta^{18}O$ for any foraminifera genera (Figure 2C). In general, we find enriched values for thermocline genera Subbotina spp. relative to mixed-layer dwelling *Acarinina* spp. and *Morozovella* spp. which is in accordance with vertical temperature gradients (Figure 2C). The onset of the CIE at ~ 204 m depth is marked by a depletion in all planktonic genera of ~1‰ (Figure 2C). $\delta^{18}O$ values recover gradually back to pre-CIE values at 191 m depth (Figure 2C).

The SDB benthic foraminifera $\delta^{13}C$ record is based on analyses of 2 taxa, and in general values closely follow the bulk curve (Figure 2B). Within the Aquia, *Cibicidoides* spp. $\delta^{13}C$ show a gradual decline until the POE where carbon $\delta^{13}C$ values show a depletion of 2‰ and then recover (Figure 2B). In the Marlboro Clay, values are based on analyses of *A. acutus* which are

abundant and display a steady recovery in $\delta^{13}C$ values back towards baseline until approximately -0.5‰ where they level out at 188 m. Mean pre-CIE and CIE "core" benthic foraminifera $\delta^{13}C$ values are 0.41‰ and -2.55‰ respectively (Figure 2B). Benthic oxygen values show no excursion at the POE. There is a steady decline in $\delta^{18}O$ values from -1.0‰ to -1.5‰ prior to the CIE. Through the CIE there is a 1.7‰ decrease with values sustained at roughly -3.0‰ for 10m through the CIE "core" followed by a steep enrichment to -1.5‰ at the recovery interval (Figure 2C). Pre-CIE and CIE "core" benthic $\delta^{18}O$ values are -1.31‰ and -3.02‰, respectively (Figure 2C).

3.2 Trace Metals- SDB

Planktonic foraminifera *Acarinina* spp. and *Subbotina* spp. Mg/Ca data show a slight rise in Mg/Ca values of 0.41 mmol/mol and 0.03 mmol/mol coincident with the POE. The sampling resolution was insufficient to capture changes in Mg/Ca for surface dwelling *Morozovella* spp. across the POE. Post-POE measurements for *Acarinina* spp. and *Subbotina* spp. show a re-equilibration back to baseline values of ~3.2 mmol/mol. This is then followed by a sharp increase in Mg/Ca values for all planktonic foraminifera at the CIE. *Acarinina* spp., *Morozovella* spp. and *Subbotina* spp. Mg/Ca values show an increase of 1.45 mmol/mol, 2.04 mmol/mol and 2.71 mmol/mol respectively (Figure 4B). Mg/Ca values decrease slightly within the CIE "core" until ~195 m and then recover back to pre-CIE values by the end of the recovery

interval.

The SDB benthic foraminifera Mg/Ca record is based on analyses of 2 taxa (Figure 4B) and in general, show similar pattern as the planktonic genera. Pre-CIE average Mg/Ca values for *Cibicidoides* spp. are 3.60 mmol/mol. Excluding the large excursion at the POE, the mean pre-CIE baseline value is lower, about 3.23 mmol/mol. From 208.1 to 205.6 m, Mg/Ca values for *Cibicidoides* spp. increase by 1.86 mmol/mol and exceed Mg/Ca at the POE for any other taxa at SDB. This is followed by a rapid decrease in Mg/Ca values just prior the CIE. The transition from *Cibicidoides* spp. to *A. acutus* at the CIE shows an excursion of ~2.17 mmol/mol. The CIE "core" is marked by shifts in benthic Mg/Ca of ~1 mmol/mol. At 197.9 m, there is a sharp decrease in *A. acutus* Mg/Ca values back to pre-CIE values and lower. Pre-CIE and CIE "core" Mg/Ca values for the benthic foraminifera studied here are 3.60 mmol/mol and 4.80 mmol/mol respectively (Figure 4B).

Benthic foraminifera B/Ca values exhibit changes that coincide with both the POE and CIE (Figure 4C). *Cibicidoides* spp. values at the POE decrease by 30 µmol/mol and then rise back to baseline values by the end of the POE. The mean pre-CIE B/Ca value for *Cibicidoides* spp. is 131 µmol/mol. The transition from *Cibicidoides* spp. to *A. acutus* is characterized by a drop in B/Ca values of 51 µmol/mol at the CIE. Up the section at the core of the CIE and into the recovery there is a general trend of increasing

B/Ca values with oscillations in B/Ca ranging from 14 to 42 μmol/mol. By the end of the PETM, B/Ca values reach pre-CIE levels of approximately 140 μmol/mol (Figure 4C).

3.3 %$CaCO_3$ and Stable Isotopes- Cam-Dor

Percent $CaCO_3$ values (Cheyne Hirota, 2015) are relatively low, ranging from <1% to 18% in accordance with other sites on the Atlantic margin. In the Aquia %$CaCO_3$ values average ~4%. At 227 m (i.e., the POE) there is a sharp decline to <1%. This is followed by a rapid increase in %$CaCO_3$. Near the top of the Aquia there is a general increase to 8%. In the transition from the Aquia to Marlboro (the CIE 224 m) %$CaCO_3$ declines sharply to 0.1%. These low values are sustained for 1.5 m gradually increasing to pre-CIE values of ~3% to 4%. At 212 m, the transition from the Marlboro to Nanjemoy, %$CaCO_3$ increases abruptly to 18% (Figure 5A).

The bulk $\delta^{13}C$ record (Cheyne Hirota, 2015) shows an initial depletion at ~227 m of about 1‰ at the POE. Values then rebound to 1‰ just prior to the CIE which is marked by a decrease of 3.86‰. The low values are maintained through the CIE "core" until 216.4 m where the recovery of carbon values back to pre-CIE values initiates with values increasing to ~0.5‰ within the Nanjemoy (Figure 5B). The bulk $\delta^{18}O$ record (Figure 5C) for Cam-Dor is highly variable with oscillations of as much as 3‰ throughout the entirety of the PETM. The CIE is characterized by an approximate 2‰ depletion in bulk

$\delta^{18}O$ with average CIE "core" values of around -2.5‰ (Figure 5B). Through the Marlboro Clay average values increase to -1.5‰ and at the contact with the Nanjemoy increase further to -1‰.

The planktonic foraminifera $\delta^{13}C$ values generally follow the bulk curve but are enriched by as much as 3‰ (Figure 5B). There is no obvious signal in planktonic foraminifera $\delta^{13}C$ values at POE intervals. Similar to SDB, Cam-Dor displays vertical isotopic gradients from surface to bottom waters with *Morozovella* spp. and *Acarinina* spp. being the most enriched. Pre-CIE averages for *Morozovella* spp., *Acarinina* spp. and *Subbotina* spp. are 3.82‰, 2.40‰ and 1.64‰ respectively (Figure 5B). At the CIE (224 m) there is a sharp depletion in all planktonic foraminifera carbon values of approximately 3.5‰. The low values are maintained through the 10 m of the Marlboro clay (Figure 5B).

Planktonic foraminifera $\delta^{18}O$ values show similar patterns to carbon values. The pre-CIE interval at Cam-Dor displays no shifts in $\delta^{18}O$ coincident with the POE for any planktonic foraminifera studied here. Pre-CIE $\delta^{18}O$ averages for *Morozovella* spp., *Acarinina* spp. and *Subbotina* spp. are -3.12‰, -2.26‰ and -2.33‰ respectively (Figure 5C). Coincident with the onset of the CIE, values for all species decline by roughly 1.0‰. These depleted values are maintained through the top of the Marlboro Clay where values return towards pre-CIE values (Figure 5C).

The benthic foraminifera isotope record is based on *Cibicidoides* in the Aquia Fm. and *A. acutus* in the Marlboro Clay. Benthic $\delta^{13}C$ tends to parallel planktonic foraminifera values with a depletion of <1‰ at the POE, and increasing slightly prior to the P-E boundary. In the Marlboro Clay, A. acutus values are about 3.5‰ lower and remain so to the top of the clay, recovering to pre-boundary values at the contact with the Nanjemoy (Figure 5B). Benthic $\delta^{18}O$ data for Cam-Dor, unlike the $\delta^{13}C$ record, displays a small depletion of <1‰ coincident with the POE. At the transition from the Aquia to the Marlboro Clay there is a ~1.8‰ (Figure 5C) depletion which is the largest depletion for any taxa at Cam-Dor. Within the Marlboro Clay there is a gradual recovery of $\delta^{18}O$ values back to pre-CIE levels in the Nanjemoy Fm. (Figure 5C).

3.4 Trace Metals- Cam-Dor

Due to the low shell abundances, shifts in Mg/Ca across the CIE could only be documented for planktonic foraminifera *Subbotina* spp. and benthic foraminifera *Cibicidoides* spp. and *A acutus.* No pre-CIE values were measured for *Morozovella* spp. and one pre-CIE value was measured for Acarinina spp. however, the full magnitude of the Mg/Ca increase was not captured. Average pre-CIE Mg/Ca values for Subbotina spp. are 2.60 mmol/mol. Across the P-E boundary, Mg/Ca increases by 1.96 mmol/mol remaining high through the Marlboro Clay, then declining to 3.42 mmol/mol

within the Nanjemoy, greater than pre-CIE values. Average CIE "core" Mg/Ca values for Subbotina spp. are 3.96 mmol/mol (Figure 6B). Benthic foraminifera at Cam-Dor display remarkable shifts in Mg/Ca and are very similar to changes observed at SDB in this study. Pre-CIE *Cibicidoides* spp. Mg/Ca values, similar to SDB show an extraordinarily large POE signal with an increase of 0.89 mmol/mol at 227 m. This is followed by a larger decrease in Mg/Ca values of 1.56 mmol/mol just prior to the CIE. The shift from *Cibicidoides* spp. to *A. acutus* at the CIE is marked by a sudden increase in Mg/Ca values of 2.40 mmol/mol at 224 m. Following this increase there is a gradual decrease to 3.48 mmol/mol (Figure 6B). No recovery Mg/Ca values were documented for benthic foraminifera at Cam-Dor.

Benthic B/Ca values display an increase at the onset of the POE at 227 m. Coincident with minimum POE depleted values (226 m), B/Ca values for Cibicidoides are ~186 µmol/mol and decrease to 114 µmol/mol just prior to the onset of the CIE. Across the transition to the Marlboro Clay, B/Ca values for A. acutus decrease to ~70 µmol/mol and remain steady throughout the entirety of the CIE "core" only displaying an increase of 28 µmol/mol at 215 m (Figure 6C).

IV. DISCUSSION

4.1 Coastal Ocean Paleotemperature

4.1.1 $\delta^{18}O$ Derived Temperature Estimates

For this study, local $\delta^{18}O$ of seawater (0.39‰ vSMOW) and oxygen temperatures were estimated using published calibrations (Zachos et al., 1994; Bemis et al., 1998; Marchitto et al., 2014) (see appendix). Absolute $\delta^{18}O$ derived temperatures at SDB for planktonic foraminifera *Morozovella* spp., *Acarinina* spp. and *Subbotina* spp. are offset, but exhibit similar warming trends (+4.5 to 6°C) across the P-E boundary. On average pre-CIE *Acarinina* spp. temperatures are just slightly higher (~31.7 °C, n=18) than *Morozovella* spp. (30.6 °C, n=8) (Figures 8 and 9B). Across the CIE *Morozovella* spp. and *Acarinina* spp. record SST rise to peak CIE "core" temperatures of 36.6 and 36.2 °C, respectively (Figures 8 and 9B). Thermocline dwelling *Subbotina* spp. temperatures reflect a deeper habitat with average pre-CIE and CIE temperatures of 25°C and 30.7 °C (Figures 8 and 9B). Benthic oxygen derived temperatures display the lowest values indicative of their bottom-water environment. Average pre-CIE and CIE "core" temperatures for *Cibicidoides* spp. and *A. acutus* are 20.8 and 31.3 °C respectively (Figures 8 and 9b). Assuming no difference in vital effects, the 10.5 °C increase in temperatures is the largest rise in temperature recorded by foraminifera in this study.

Estimated O-temperatures at Cam-Dor show very similar patterns to that of SDB. Surface dwelling foraminifera *Morozovella* spp. yields average

pre-CIE temperatures of 32.0 °C (Figures 8 and 10B) rising to 35.7 °C in the CIE "core". Pre-CIE *Acarinina* spp. based temperature estimates are highly variable with values ranging from 25.0 to 32.0 °C (Figures 8 and 10B). The temperatures increase to 33.4°C within the CIE (Figures 8 and 10B). Pre-CIE *Subbotina* spp. derived temperatures are 25.0 °C increasing to 30.1 °C within the CIE (Figures 8 and 10B). Similar to SDB, benthic foraminifera at Cam-Dor show the largest increase in temperatures for any genera at this site. Pre-CIE average bottom water temperatures are 21.1 °C as estimated from *Cibicidoides* spp (Figures 8 and 10B) increasing to 30.6 °C in the CIE "core" as estimated from *A. acutus* (Figures 8 and 10B).

4.1.2 Mg/Ca Derived Temperature Estimates

Mg/Ca planktonic temperature estimates are based on the Evans and Müller (2012) calibration with exponential constants A and B of Anand and Elderfield (2003) (see appendix). We elected to use the latter constants because the temperatures were derived from the $\delta^{18}O$ of the same shells rather than climatological SST, an approach that seems more appropriate for application to paleostudies.

In general, the Mg/Ca temperatures for both planktonic surface dwelling taxa *Acarinina* spp. and *Morozovella* spp. at SDB are similar to those estimated from O-isotopes. This close agreement reveals that Mg/Ca temperature estimates are fairly well constrained and allow for accurate SSS

estimates. Pre-CIE Mg/Ca based temperatures for mixed layer foraminifera *Acarinina* spp. and *Morozovella* spp. at SDB average 28.8 and 29.1 °C, increasing by 2.3 and 4.3 °C through the CIE respectively (Figures 8 and 9C). The pre-CIE temperature estimate for Subbotina is 28.9 °C, which is somewhat warmer than estimated with O isotopes, increasing by 3.2 °C to 32.2 °C within the CIE (Figures 8 and 9C).

Mg/Ca temperature calibrations for shallow water benthic genera are uncommon; most of the past calibration work has focused on deep-sea benthic taxa. Several calibration studies of pelagic benthics are considered for temperature determination for this study including Lear et al. 2002, Elderfield et al. 2006, and Marchitto et al. 2007 (see appendix). Due to a closer agreement with oxygen temperature estimates, we apply the calibration of Marchitto et al. 2007 to compute the benthic temperatures on the mid-Atlantic shelf (see appendix). As such, the error on our absolute temperature estimates is likely quite large, on the order of ± 3 to 5°C given the lack of a modern calibration for shallow marine benthic taxa. Indeed, the range in calibrations for benthic foraminifera is quite large between pelagic and shallow water taxa of >20°C. The error on the P-E anomaly is likely smaller, just ±2-3°C assuming the relative sensitivity of Mg/Ca to T is roughly the same as with modern pelagic ancestors.

At SDB the coupled *Cibicidoides* spp. and *A. acutus* Mg/Ca record

yields the largest temperature increase of the taxa examined across the P-E boundary. The average pre-CIE temperature based on Mg/Ca of *Cibicidoides* spp. is ~21°C (Figures 8 and 9C). Based on the mean *A. acutus* values we estimate a 7.8 (±2.5) °C rise into the Marlboro Clay (Figures 8 and 9C). Temperatures remain elevated through most of the Early Eocene in the Marlboro Clay and fall gradually to pre-CIE temperatures within the Nanjemoy Fm. (Figure 9C).

The Cam-Dor Mg/Ca based temperature records are not as complete as SDB due to low abundances of foraminifera. As a consequence, the full magnitude of temperature change at the onset of the PETM could not be determined for either of the mixed-layer foraminifera taxa. Late Paleocene *Acarinina* spp. yield Mg/Ca temperatures of ~29°C. Thermocline dwelling Subbotina spp. Mg/Ca based temperatures are about 2 °C cooler than SDB. The average pre-CIE Mg/Ca temperature at Cam-Dor is ~26 °C in the Aquia Fm. Into the Marlboro Clay there is ~5 °C rise in temperatures with CIE "core" temperatures averaging ~30 °C (Figures 8 and 9C). Finally, benthic temperatures at Cam-Dor are 5 °C cooler relative to benthic genera at SDB. Within the latest Paleocene Aquia Fm., average *Cibicidoides* spp. temperatures are approximately 15 °C. Across the CIE into the Marlboro clay there is an 8 °C rise in bottom water temperatures which is an approximately 1 °C smaller increase than that of SDB. Average CIE "core temperatures for

A. acutus are 23.3 °C (Figures 8 and 9C).

4.2 Salinity Changes on the Shelf

Certain factors can confound estimates of temperature by $\delta^{18}O$. In particular, changes in local salinity, can skew the $\delta^{18}O$ and temperature relationship. However, if temperature can be constrained with an independent proxy, such as Mg/Ca, it should be possible to compute the relative changes in local salinity, a potentially valuable climate parameter. As mentioned earlier, the PETM on the mid-Atlantic shelf is marked by an increase of freshwater input onto the shelf at the onset of the CIE (Gibson et al., 2000; Self-Trail et al. 2017). Given that local freshwater has a much lower $\delta^{18}O$ (~-5 to -7‰) than sea water (Roberts et al., 2011), it would be expected that a major freshening event such as the PETM would artificially deplete the local $\delta^{18}O$ of seawater, thus providing an opportunity to estimate local salinity changes on the shelf throughout the event.

A cross plot of $\delta^{18}O$ derived temperatures versus Mg/Ca derived temperatures for pre-CIE and CIE “core” intervals for each genera (Figure 8) analyzed in this study can be used to identify a potential salinity effect. Hypothetically, if there were no confounding factors influencing $\delta^{18}O$ or Mg/Ca other than temperature, it would be expected that the slope of the $\delta^{18}O$ and Mg/Ca temperature regressions for each genera to be 1:1. We find, however, the $\delta^{18}O$ derived changes in temperature are consistently larger than Mg/Ca

indicating that local salinity is changing on the shelf and in turn influencing local $\delta^{18}O$ of sea water (Figure 8).

With the onset of the CIE, sea surface salinity as derived from *Acarinina* spp. at SDB indicates a major freshening event where sea surface salinity decreased by as much as 4 psu (Figure 11). This is in agreement with (Pagani et al. 2006; Kopp et al. 2009) which argue that an enhanced hydrologic cycle at the onset of the PETM would have caused the formation of a fresh water lens at the surface. Within the earliest Eocene Marlboro Clay, the CIE "core" displays an increase towards more saline conditions. By the recovery interval of the Nanjemoy Fm. sea surface salinity returns to baseline pre-event values (Figure 11).

Sea surface salinity trends as inferred from the $\delta^{18}O$ and Mg/Ca of *Acarinina* spp. at Cam-Dor are remarkably similar to that of SDB. With baseline upper Paleocene values, (set at 224 m), the onset of the CIE is marked by a freshening of as much as 3 psu within the Marlboro Clay (Figure 12). In the recovery interval salinity values return back to pre-CIE levels.

The O-isotope evidence for reduced salinity in Maryland is robust and is consistent with other evidence such as the increased flux of siliciclastics, increased abundances of brackish water taxa, and evidence for eutrophication (Lippert and Zachos, 2007; John et al., 2008; Kopp et al., 2009; Sluijs et al., 2009). Indeed, Zachos et al., (2006) used coupled

temperature proxies TEX_{86} as well as $\delta^{18}O$ to calculate relative changes in salinity at Wilson Lake through the PETM and found evidence for higher runoff and lower salinity at the onset of the event. They claim, however, that the changes in salinity were likely seasonal, possibly associated with a short but intense wet season. In this way, local relative salinity changes can be calculated for both sites SDB and Cam-Dor (for salinity estimation procedures see appendix).

4.3 Changes in Vertical Isotopic Gradients

Similar to pelagic sections, the foraminifera isotopic records at SDB and Cam-Dor show a vertical (e.g. surface to bottom) gradient. The $\delta^{13}C$ trends display enriched surface relative to depleted bottom waters. This gradient is a consequence of the preferential uptake and transfer of $\delta^{13}C$ via the biological pump (Makarova et al., 2017). The foraminifera $\delta^{18}O$ values display a reversed (low to high) gradient attributable to the vertical temperature gradient of the water column.

A potentially important feature of the climatic response documented at New Jersey P-E sections Millville and Ancora, is a weakening of the vertical $\delta^{18}O$ gradients at the onset of the PETM (Makarova et al. 2017). The difference between the $\delta^{18}O$ values of surface dwelling foraminifera and benthic foraminifera decreases with greater negative $\delta^{18}O$ excursions in thermocline and benthic foraminifera. Makarova et al., (2017) provide two

potential scenarios to explain the change in gradients. The first scenario assumes the changes in $\delta^{18}O$ for each genera are derived purely through changes in temperature of the water column, and thus the taxa's preferred depth habitat. If this were the case then $\delta^{18}O$ derived temperatures show a larger increase in bottom waters relative to surface waters. This would be consistent with a local weakening of the thermal stratification of the water column on the shelf associated with greater heating of local bottom waters. I propose that such heating would be a consequence of a reduction in meridional thermal gradients as areas of high latitude bottom water formation are preferentially warmed (i.e., polar amplification). In Scenario 2 changes in the isotopic composition of each genera are attributed to changes in either the season of calcification or the depth at which they calcify. If so, this would complicate attempts to quantify the relative changes in water column temperature as shifting planktonic foraminifer depth habitats would work to effectively dampen the magnitude of temperature change across the CIE. Foraminifera might change their depth habitat in response to certain environmental stressors (ie. salinity, pH and temperature). Surface dwelling foraminifera specifically can migrate deeper to seek refuge from warmer temperatures that might inhibit calcification (Bijma et al., 1990). The other possibility is that in response to warming at the onset of the PETM, foraminifera are changing their dominant season of calcification to cooler months (winter/spring). This would have the same effect of dampening the

magnitude of temperature change as a shift in depth habitat would. Markarova et al., (2017) argue against a change in the depth habitat of the foraminifera across the CIE based on the fact that there appears to be no change in $\delta^{13}C$ isotopic gradients, and concludes that the major driver of changes in observed isotopic compositions at Millville and Ancora are due to changes in sea water temperature. However, it is acknowledged that a change in foraminifera blooming season is also possible.

In this regard, the data from SDB and Cam-Dor provide important additional insights into the thermal evolution of the water column along the coast through the PETM. To assess relative changes in gradients, the difference (i.e., the big delta, Δ) between surface and benthic foraminifera $\delta^{13}C$ values are cross plotted against the difference between surface and benthic foraminifera $\delta^{18}O$ values at each site. The Δ between the isotopic compositions of surface and benthic foraminifera describes the state of the water column at three time intervals: pre-CIE, CIE "core" and Post-PETM. In $\delta^{18}O$ space, there is a reduction in the difference between surface and benthic foraminifera at the onset of the CIE for both SDB and Cam-Dor. At SDB, the pre-CIE $\delta^{18}O$ gradient is 1.7 ‰. Across the CIE this gradient is reduced to approximately 1.0 ‰ (Figure 13). Similar trends are seen at Cam-Dor. The pre-CIE $\delta^{18}O$ gradient is 1.9 ‰ and across the CIE this gradient is reduced to approximately 0.9 ‰ (Figure 13). The interesting characteristic of these sites and where isotopic patterns diverge from those of Millville and

Ancora is in $\delta^{13}C$ trends. The crux of Makarova et al., (2017) argument for why foraminifera do not appear to be migrating vertically is that the $\delta^{13}C$ gradients are not changing. At SDB and Cam-Dor, this is not the case. In $\delta^{13}C$ space at SDB, there is a reduction in isotopic gradients from 2.6 ‰ to 1.7 ‰ from pre-CIE to CIE "core" intervals respectively (Figure 13). At Cam-Dor there is a smaller change in $\delta^{13}C$ gradients. The pre-CIE $\delta^{13}C$ gradient is 2.7 ‰ and across the CIE to CIE "core" intervals it is reduced to 2.4 ‰ (Figure 13). Because of this change in both $\delta^{18}O$ and $\delta^{13}C$, we cannot necessarily reject the hypothesis that foraminifera at SDB and Cam-Dor are migrating vertically, thus dampening the magnitude of temperature change. Similar trends have been documented at other sites associated with PETM. For example, records of foraminifera C and O isotopes of the PETM interval in the tropical Pacific suggest mixed-layer taxa descended in the water column in direct response to warming (Kelly et al., 1996; Luciani et al., 2017).

4.4 Isotopic & Hydrographic Variation on the Shelf

Given the anomalous changes in both $\delta^{18}O$ and $\delta^{13}C$ isotopic gradients, is it possible hydrographic variation along the shelf contributed? A reduction in not only $\delta^{18}O$ but also $\delta^{13}C$ isotopic gradients as observed in Maryland sites SDB and Cam-Dor could indicate that coastal waters were more weakly stratified at northerly sites such as Millville and Ancora where $\delta^{13}C$ isotopic gradients are preserved. If we are to assume that there was no

vertical migration of foraminifera as documented at Millville and Ancora, a decrease in $\delta^{13}C$ isotopic gradients can be achieved via coastal upwelling. In addition to environmental changes already discussed, changes in wind patterns at the onset of the PETM could have initiated upwelling along the Maryland coast that would bring more depleted ($\delta^{13}C$) bottom waters closer to the surface thus weakening the $\delta^{13}C$ stratification seen in pre-CIE intervals. These upwelling patterns could perhaps be seasonal and therefore difficult to resolve given the resolution of sediment deposition on the shelf. Modeling changes in wind patterns on the mid-Atlantic shelf across the PETM could help elucidate the potential for wind driven upwelling during the PETM and should be a focus of future modeling studies.

Changes in water column density associated with hyperpycnal flow could also decrease vertical $\delta^{13}C$ isotopic gradients. Evidence for hyperpycnal flow on the shelf has been documented in western Maryland site Mattawoman Creek Billingsley-Road (MCBR) (Self-Trail et al., 2017) which would have been proximal to the paleodelta. Episodic hyperpycnal flow would have brought in fresh water to the basin floor effectively inducing inverse salinity stratification on shallower portions of the shelf during the PETM. This inverse salinity stratification could have initiated a density driven turnover of the water column, bringing older and more depleted bottom water closer to the surface, effectively lowering the $\delta^{13}C$ of the mixed layer and dampening $\delta^{13}C$ isotopic gradients on the shelf. Of course, this brings into question why hydrographic

differences exist at all between sites in New Jersey and Maryland.

One of the most important controls on coastal hydrography is the proximity to the main drainage system on the mid-Atlantic shelf. As mentioned earlier, the onset of the PETM brought about large changes to the global hydrologic cycle. The paleo-Susquehanna was particularly active during the late Paleocene and early Eocene and is considered the major drainage system along the shelf. Locally, the mid-Atlantic shelf experienced an enhanced hydrologic cycle producing large scale runoff of a magnitude to which only the modern-day Amazon River system is comparable (Kopp et al., 2009). Thus, the proximal sites to the delta (SDB and Cam-Dor) should have been affected ($\delta^{18}O$) to a larger degree than distal sites (Ancora and Millville) and may explain why isotopic patterns differ from New Jersey to Maryland sites. Comparison of cross plots of carbon and oxygen data from SDB (Figure 14) with those from New Jersey sites Bass River and Wilson lake show slightly more depleted oxygen values at peak CIE onset depth intervals within the Marlboro Clay. These depressed $\delta^{18}O$ values at SDB relative to New Jersey sites could perhaps reflect an increase in freshwater discharge at the onset of the PETM due to its proximity to the main drainage system in the area. This increase in freshwater effectively drove down the local $\delta^{18}O$ of seawater affecting the isotopic values of the foraminifera calcite.

Pre-CIE intervals for sites on the mid-Atlantic margin display a $\delta^{18}O$ gradient from north to south with more southern sites SDB and Cam-Dor

having more depleted values than northern sites Bass River and Wilson Lake (Figure 14). If it is assumed that the pre-CIE $\delta^{18}O$ of local seawater is not strongly influenced by runoff but by temperature then the gradient in $\delta^{18}O$ from north to south seen here could be attributed to meridional temperature gradients. This is supported to some extent by Mg/Ca data which consistently produce temperatures several degrees warmer when comparing Maryland sites SDB and Cam-Dor against Mg/Ca derived temperatures from New Jersey site Bass River.

V. Conclusion

Through the use of both stable isotopes and trace metal data, we have presented findings that shed light on the environmental similarities and differences between various sites on the North American mid-Atlantic shelf during the PETM. Specifically, Maryland sites SDB and Cam-Dor display similar $\delta^{13}C$ trends to New Jersey sites in the bulk and foraminifera isotopic data with excursion magnitudes of ~4 ‰. Additionally, temperatures derived from independent temperature proxies $\delta^{18}O$ and Mg/Ca allow us to roughly constrain relative changes in salinity throughout the entirety of the PETM. In agreement with the increase in flux of terrigenous material to the shelf, coupled oxygen and Mg/Ca data reveal a decrease in salinity at the onset of the CIE coincident with an expected enhancement in the hydrologic cycle. An increase in freshwater flux to the shelf would decrease local $\delta^{18}O_{sw}$ affecting

the isotopic composition of foraminifera calcite.

An interesting aspect of isotopic trends for sites in New Jersey is a larger $\delta^{18}O$ excursion recorded in benthic foraminifera, resulting in an apparent break down in vertical temperature gradients on the shelf. Due to the lack of a similar break down in $\delta^{13}C$ gradients, a change in planktic depth habitat can be ruled out. However, at sites SDB and Cam-Dor the breakdown in both $\delta^{18}O$ and $\delta^{13}C$ gradients means we cannot rule out a migration of surface dwelling foraminifera to deeper water habitats and in fact may have occurred at Maryland sites.

The apparent isotopic differences observed between New Jersey and Maryland sites begs the question; what is the source of variation on the shelf? Perhaps the main driver of hydrographic variation is the main drainage system in the area. An enhanced hydrologic cycle at the onset of the PETM drove large changes in both local $\delta^{18}O_{sw}$ and salinity on the continental margin. Proximal sites would have experienced these shifts to a greater degree than more distal sites in New Jersey. Evidence for coastal acidification is also present on the shelf and the future interpretation of B/Ca data presented here could help to confirm this.

Finally, most of the previous work on the PETM has been on open ocean pelagic sections which capture global changes in carbon cycling and large-scale fluctuations in climate. Coastal sections, on the other hand, are

influenced by a terrestrial component and can help discern more local environmental changes on the shelf during the PETM. Therefore, sites on the North American mid-Atlantic margin like SDB and Cam-Dor can provide some insight into potential local environmental changes associated with anthropogenic climate change. The proximity of coastal ocean habitats to major population centers makes it important to monitor climate change not only in the present but also in the past and the PETM is perhaps the best analog for understanding this.

Figures

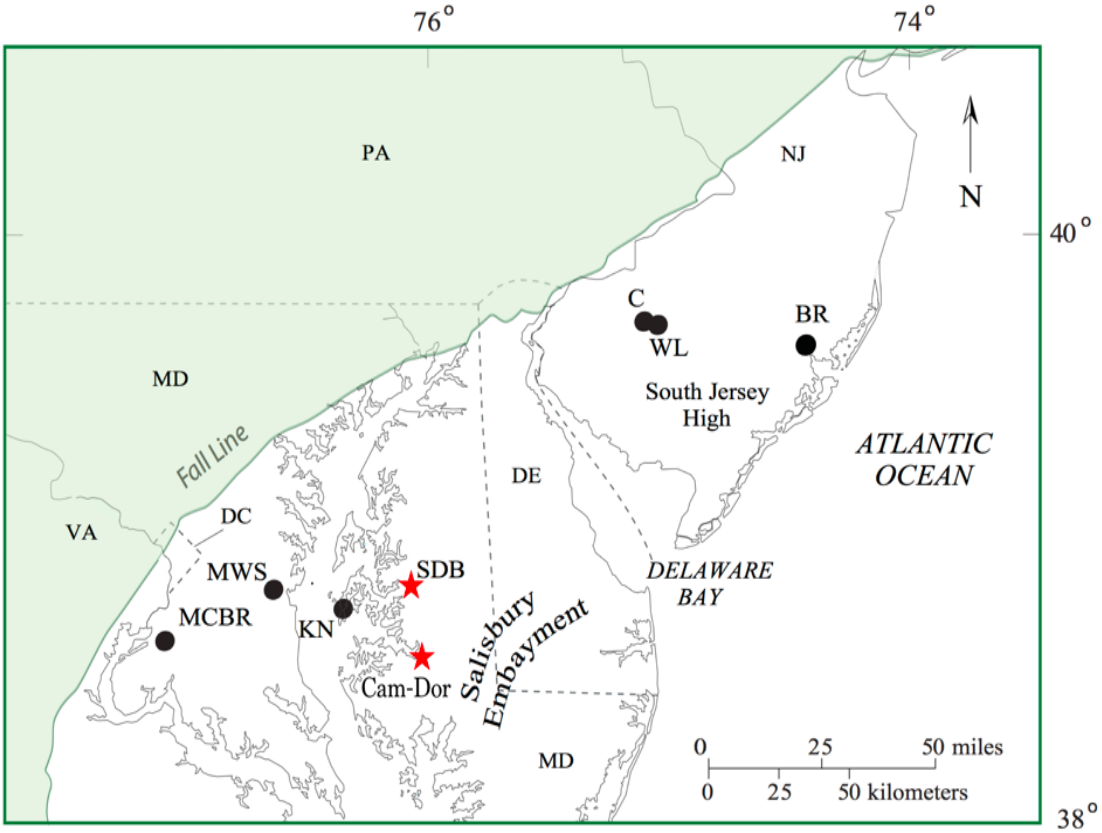

Figure 1: Locations of all drill cores spanning the Paleocene-Eocene boundary within the Salisbury Embayment. Sites SDB and Cam-Dor (red star symbol) were sampled for this study. The other locations; C= Clayton; A= Ancora; WL= Wilson Lake; BR= Bass River; MV= Millville; SDB= South Dover Bridge; Cam-Dor= Cambridge-Dorchester; KN= Knapps Narrows; MSW= Merkle Wildlife Sanctuary; MCBR= Mattawoman Creek-Billingsley Road. Modified from Self-Trail et al. 2012.

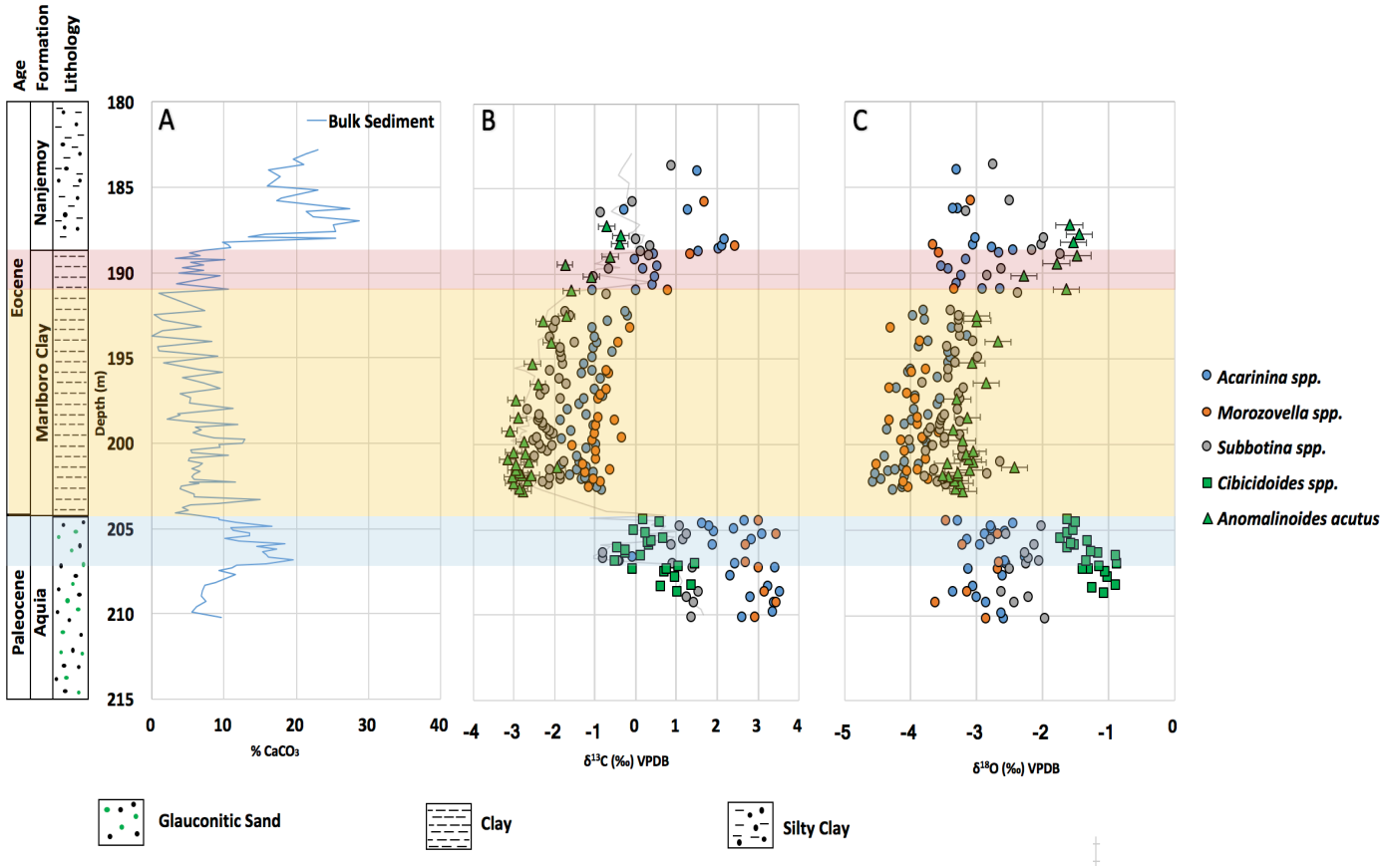

Figure 2: South Dover Bridge (SDB) %$CaCO_3$ (courtesy J. Self-Trail) and stable C and O isotope data (P.F. data courtesy of T. Babila unpublished) plotted versus depth. **A**: %$CaCO_3$ of bulk sediment. **B**: Multi-shell foraminifera $\delta^{13}C$ data. **C**: Multi-shell foraminifera $\delta^{18}O$ data. Shaded bands denote respective phases of the PETM event as represented by the CIE, the onset, core, and recovery.

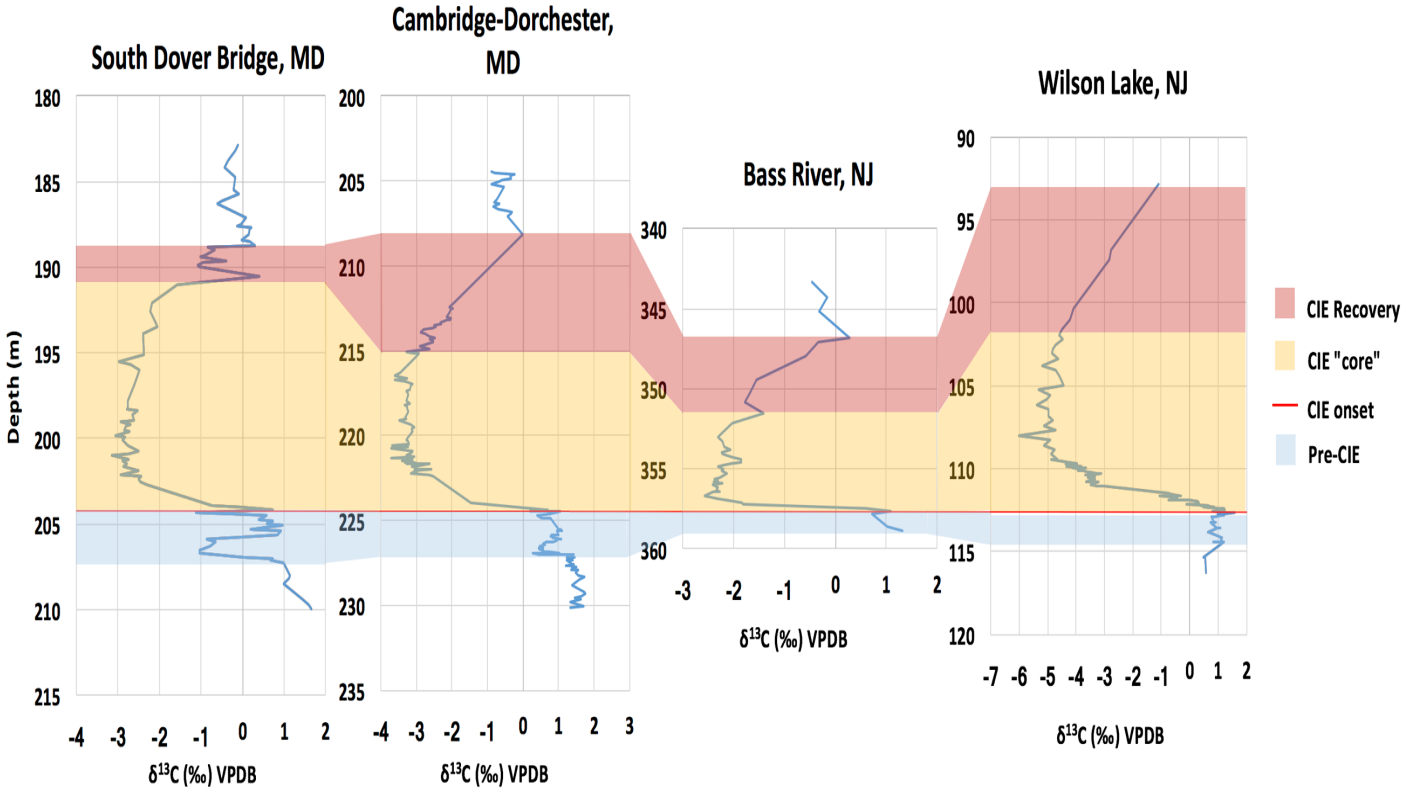

Figure 3: Graphic correlation of bulk $\delta^{13}C$ records from South Dover Bridge, Cambridge-Dorchester, Bass River, and Wilson Lake. Shaded bands denote respective phases of the PETM event as represented by the CIE, the onset, core, and recovery.

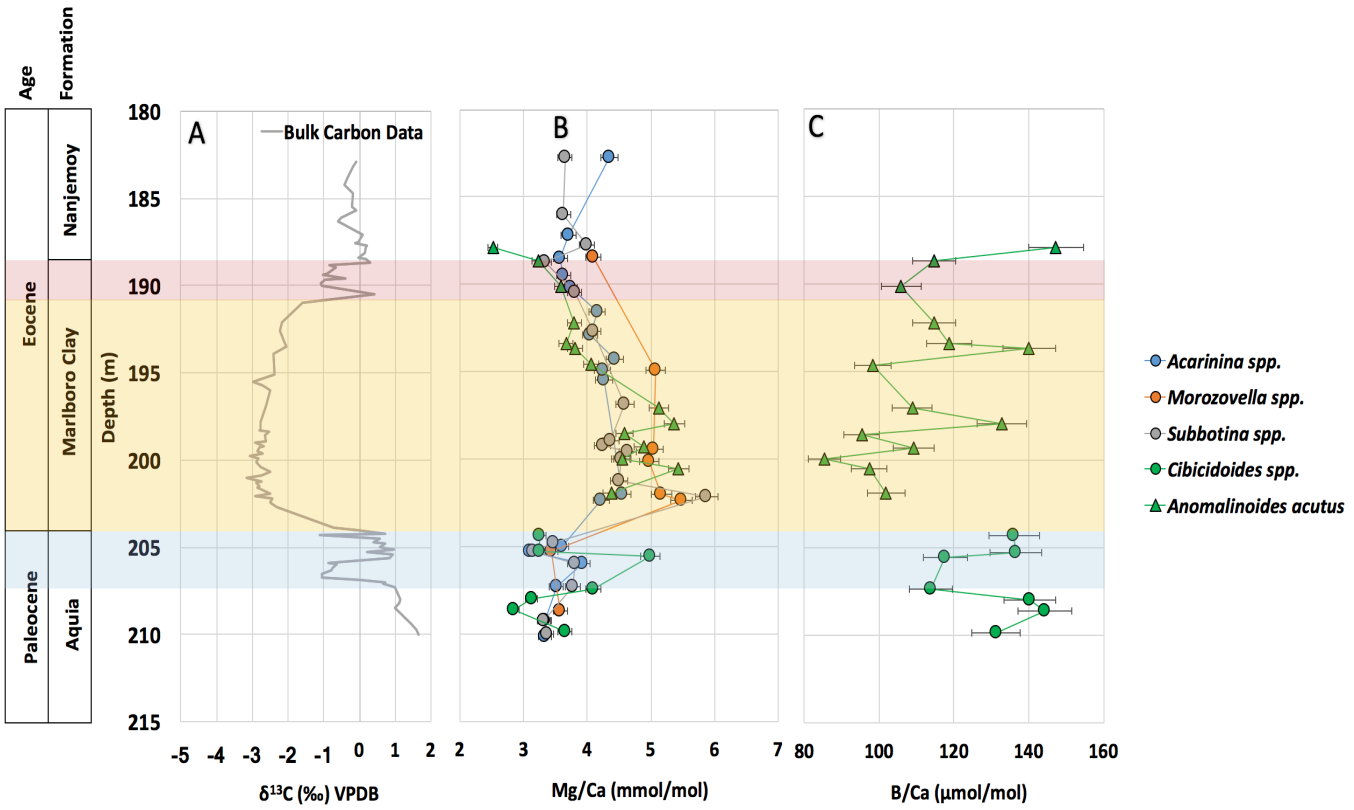

Figure 4: **South Dover Bridge** Bulk $\delta^{13}C$ and foraminifera trace metal data plotted versus depth (m) over the upper Paleocene and lower Eocene. **A**: $\delta^{13}C$ of bulk sediment. **B**: Multi-shell foraminifera Mg/Ca data (P.F. data courtesy of T. Babila unpublished). **C**: Foraminifera B/Ca data. Shaded bands denote respective phases of the PETM event as represented by the CIE, the onset, core, and recovery.

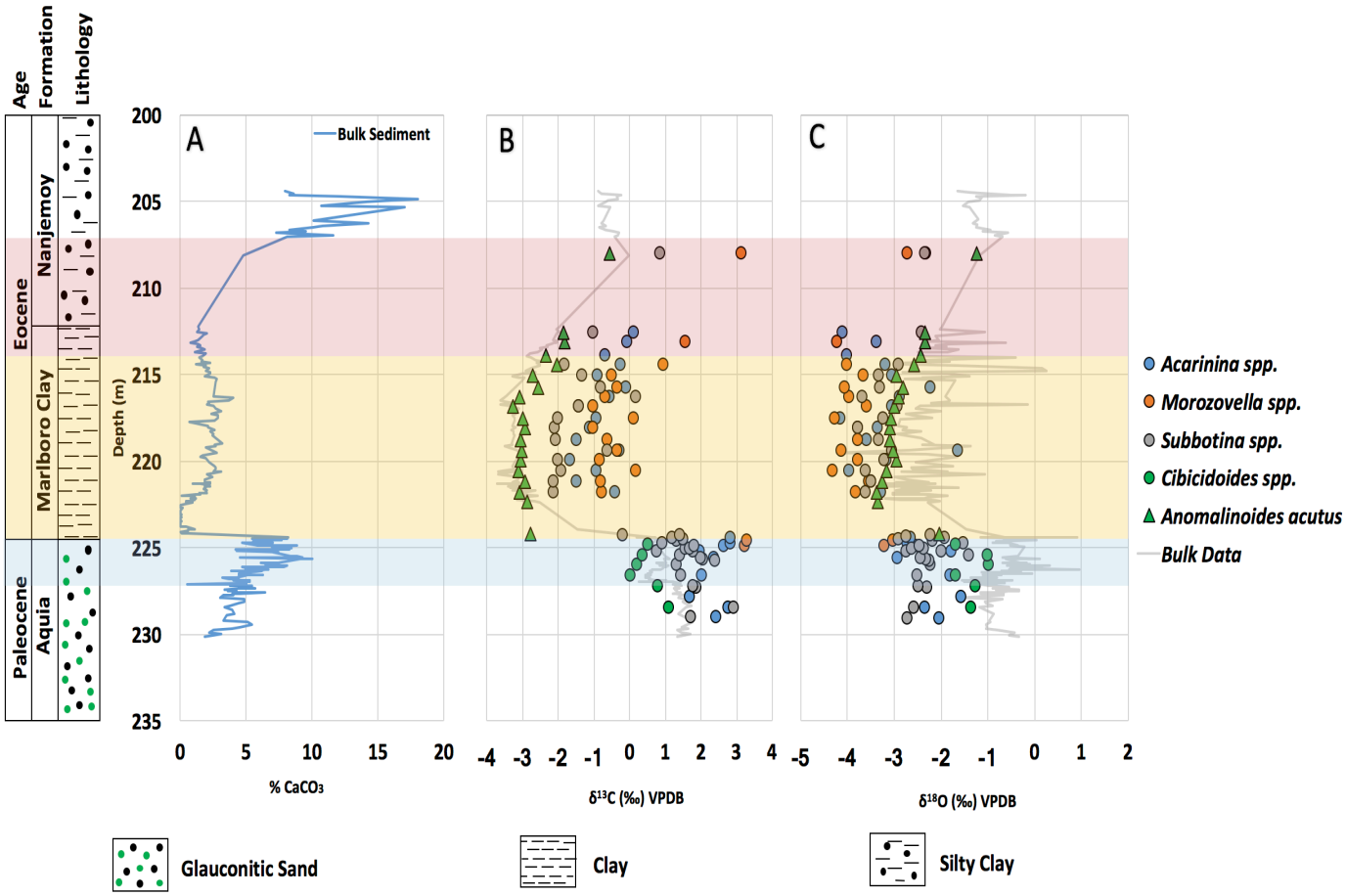

Figure 5: Cam-Dor %$CaCO_3$ and stable isotope data plotted versus depth (m) over the upper Paleocene and lower Eocene. **A**: %$CaCO_3$. **B**: Multi-shell foraminifera $\delta^{13}C$ data. **C**: Multi-shell foraminifera $\delta^{18}O$ data.

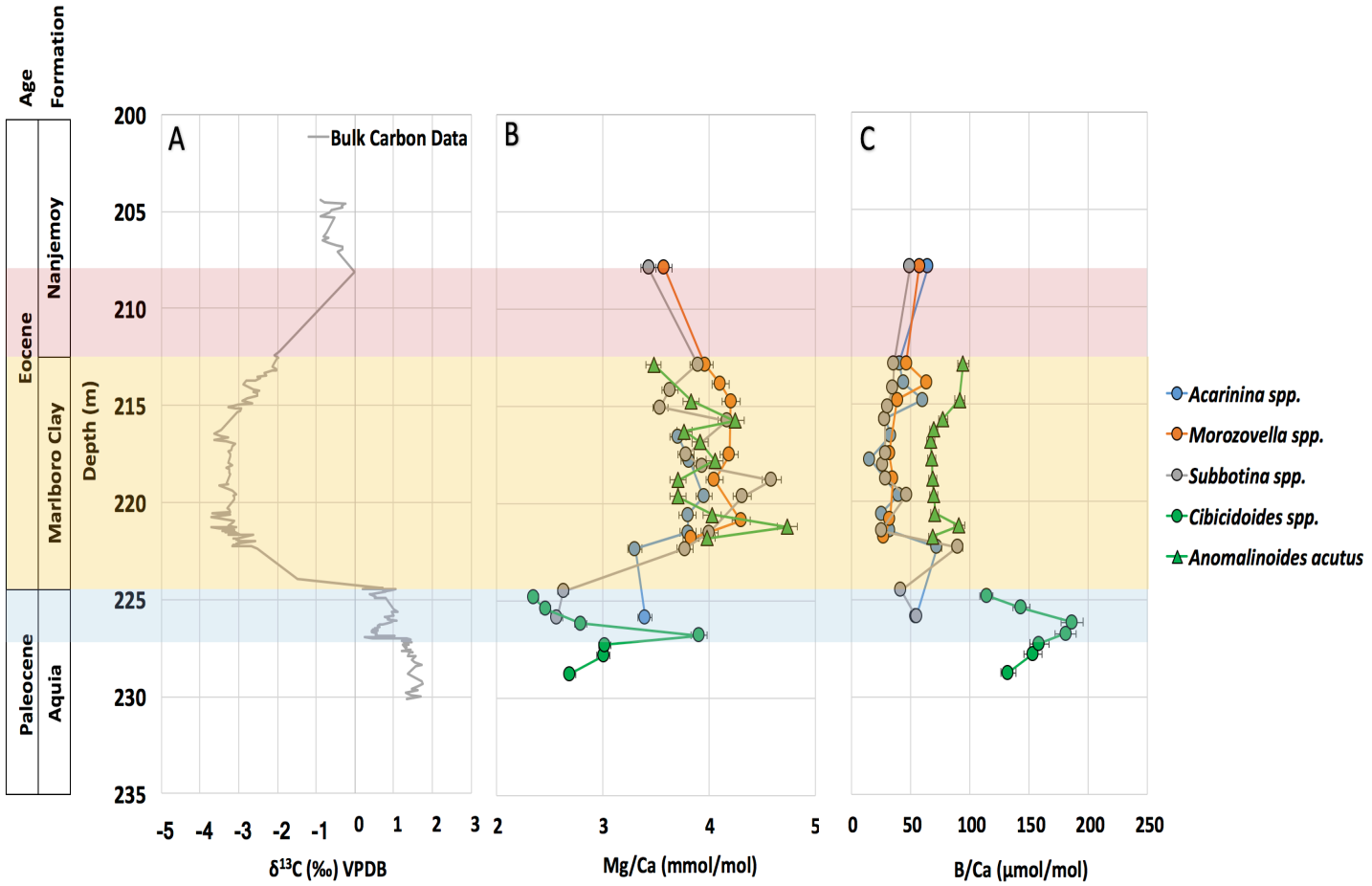

Figure 6: Cam-Dor C isotope and trace metal data plotted versus depth (m). **A**: Bulk sediment $\delta^{13}C$. **B**: Foraminifera Mg/Ca (mmol/mol). **C**: ICP-MS Foraminifera B/Ca (umol/mol).

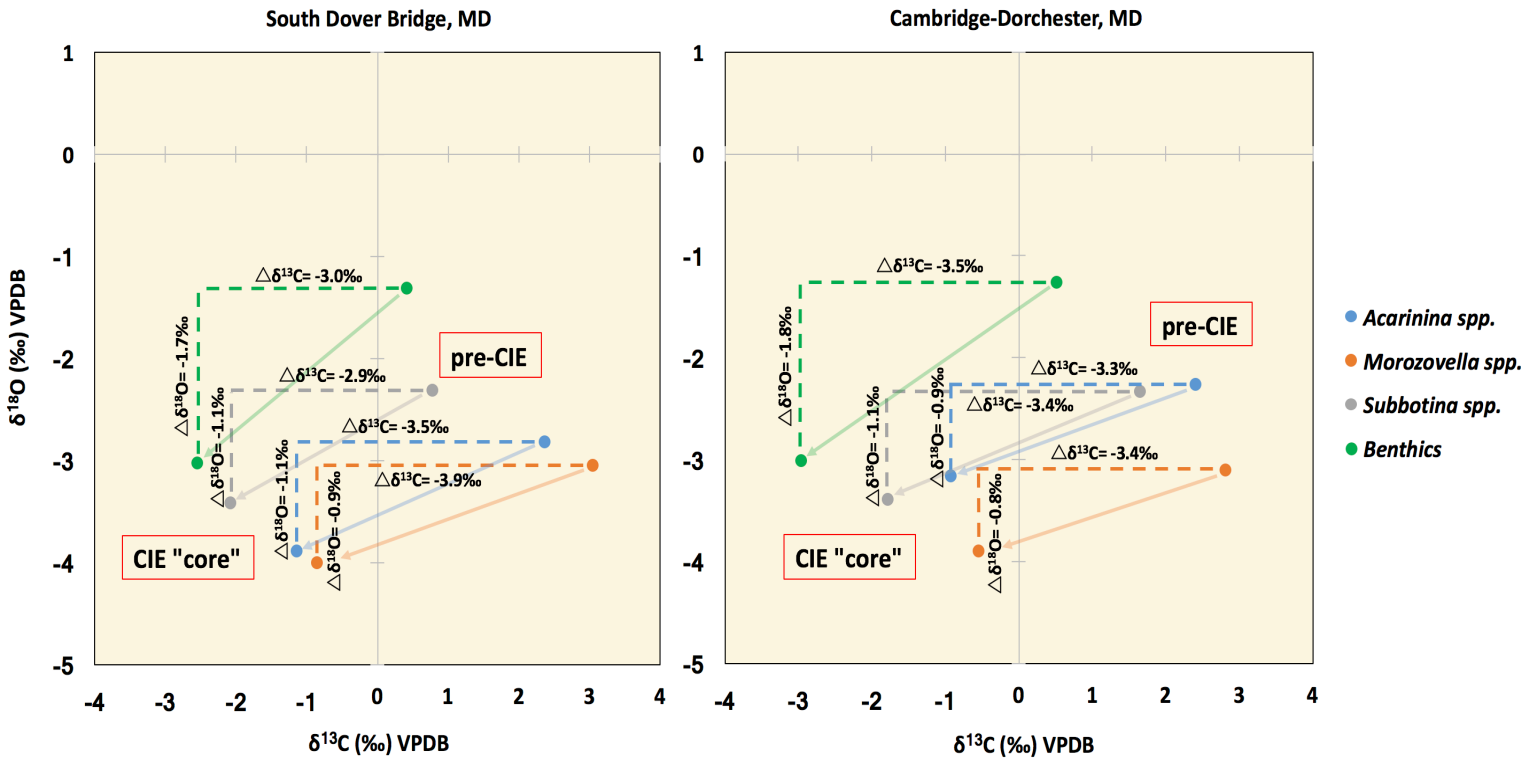

Figure 7: Cross plot of $\delta^{13}C$ and $\delta^{18}O$ data from sites SDB and Cam-Dor. Each data point represents an average isotopic value for each foraminifera genera in either pre-CIE or CIE "core" intervals.

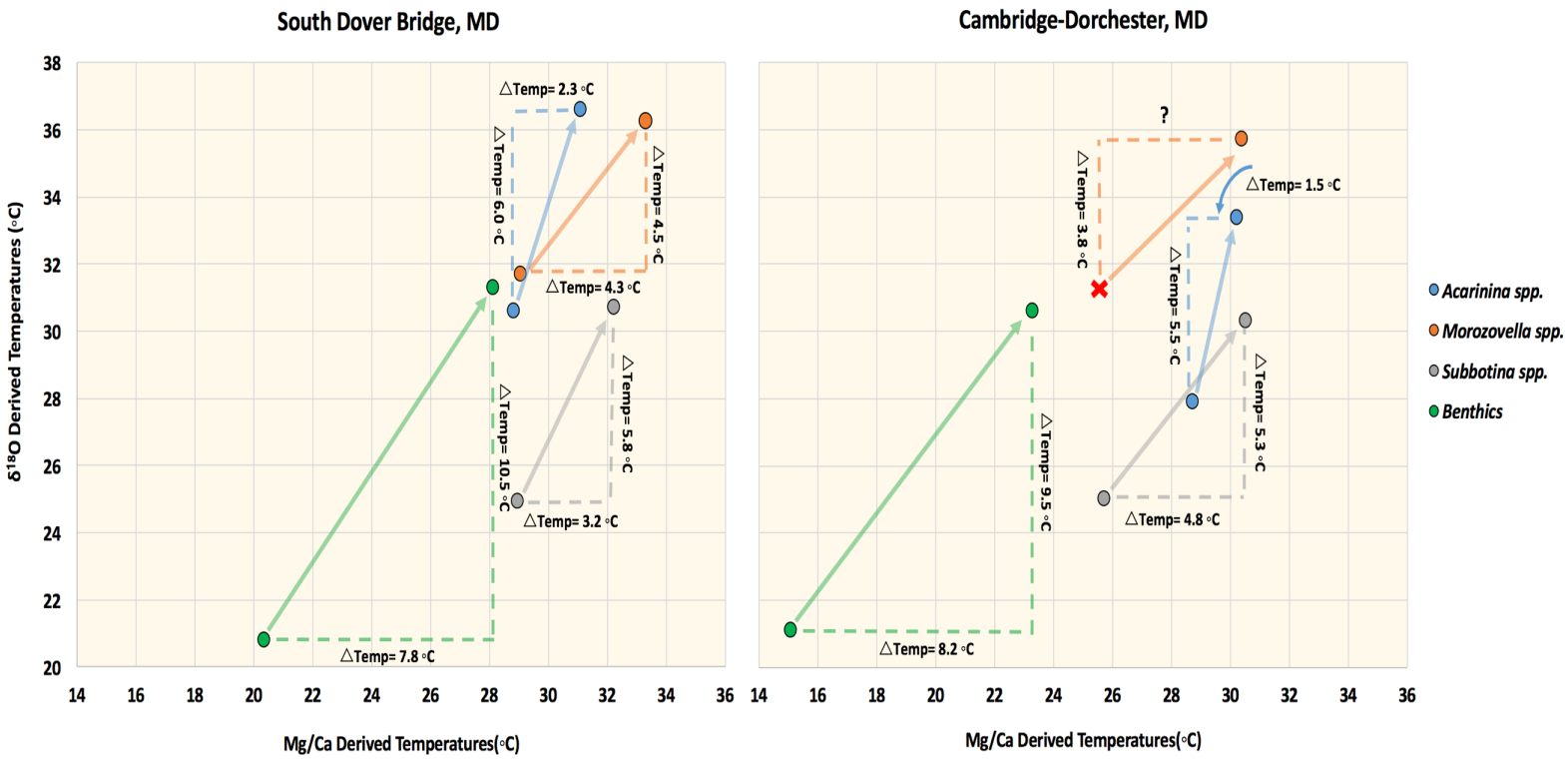

Figure 8: Cross plot of $\delta^{18}O$ and Mg/Ca derived temperatures from sites SDB and Cam-Dor. Each data point represents an average temperature for each foraminifera genera in either pre-CIE or CIE "core" intervals. Plotted are the changes in $\delta^{18}O$ and Mg/Ca derived temperatures across the CIE. The red "x" indicates that no Mg/Ca pre-CIE values for *Morozovella* spp. were measured.

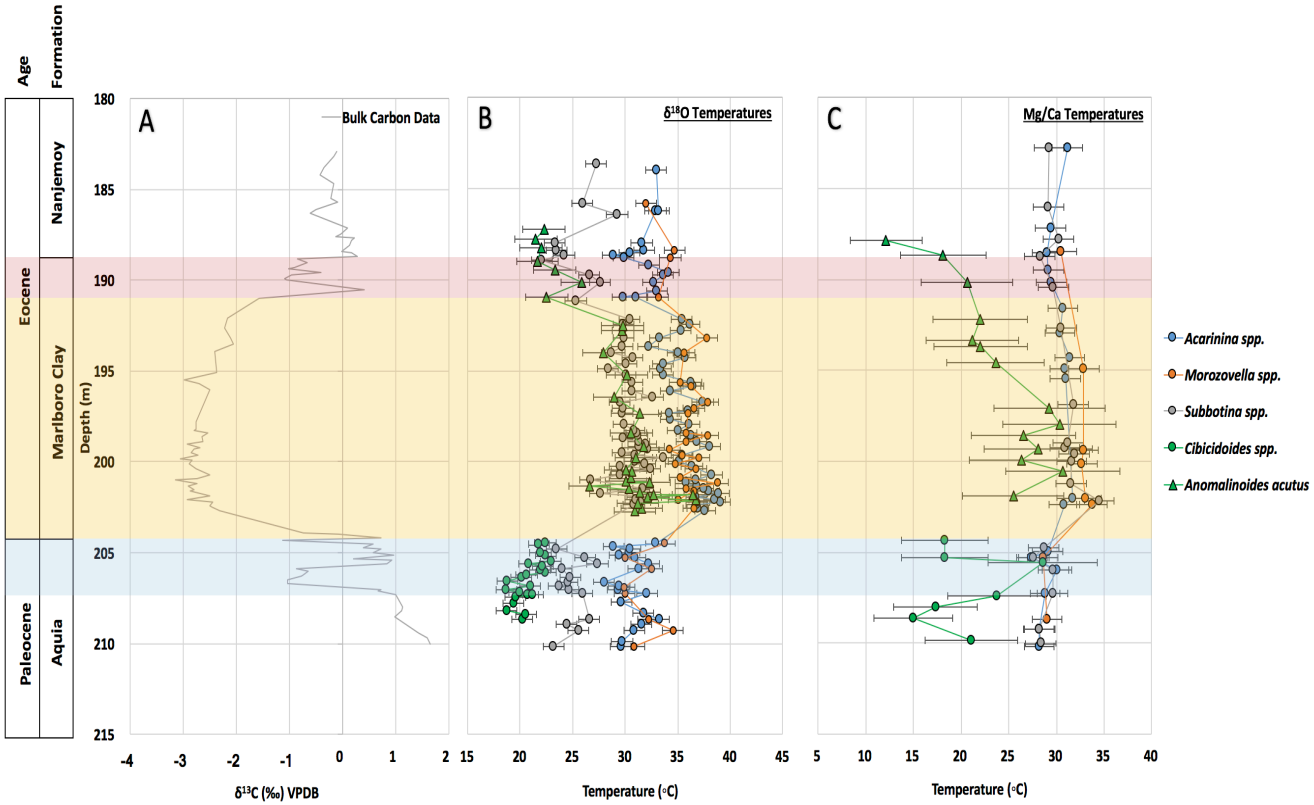

Figure 9: South Dover Bridge bulk $\delta^{13}C$ and foraminifera $\delta^{18}O$ and Mg/Ca based temperature estimates plotted versus depth. **A**: $\delta^{13}C$ for bulk sediment. **B**: $\delta^{18}O$ derived temperatures (°C) from multi-shell foraminifera data. **C**: Mg/Ca derived temperatures from ICP-MS foraminifera data. Colors represent pre-CIE, CIE "core" and recovery intervals

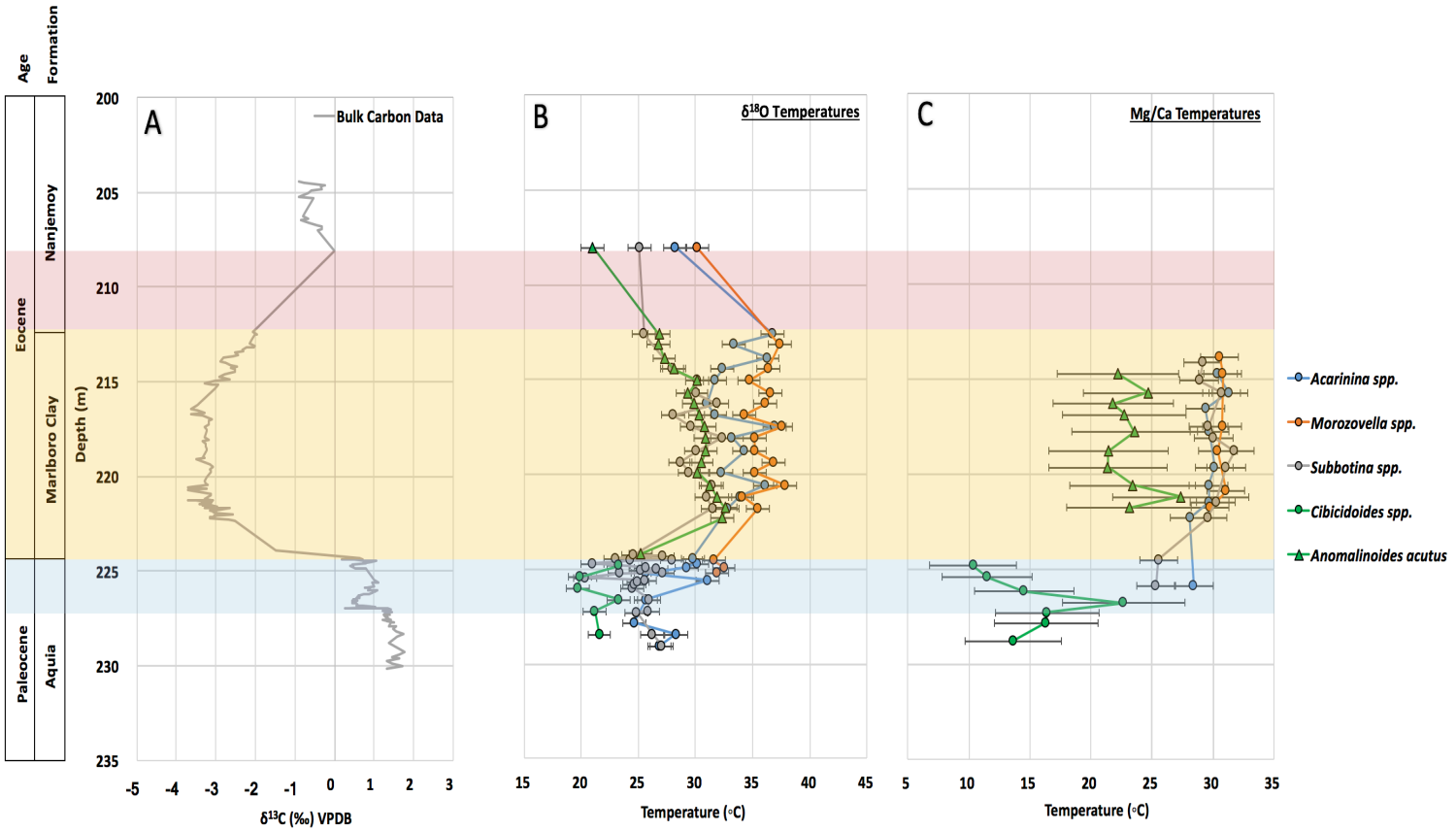

Figure 10: Cam-Dor bulk $\delta^{13}C$ and temperature plotted versus depth. **A**: $\delta^{13}C$ data as measured from bulk sediment for reference. **B**: temperatures as estimated from $\delta^{18}O$ of multi-shell foraminifera. **C**: temperatures as estimated from foraminifera Mg/Ca.

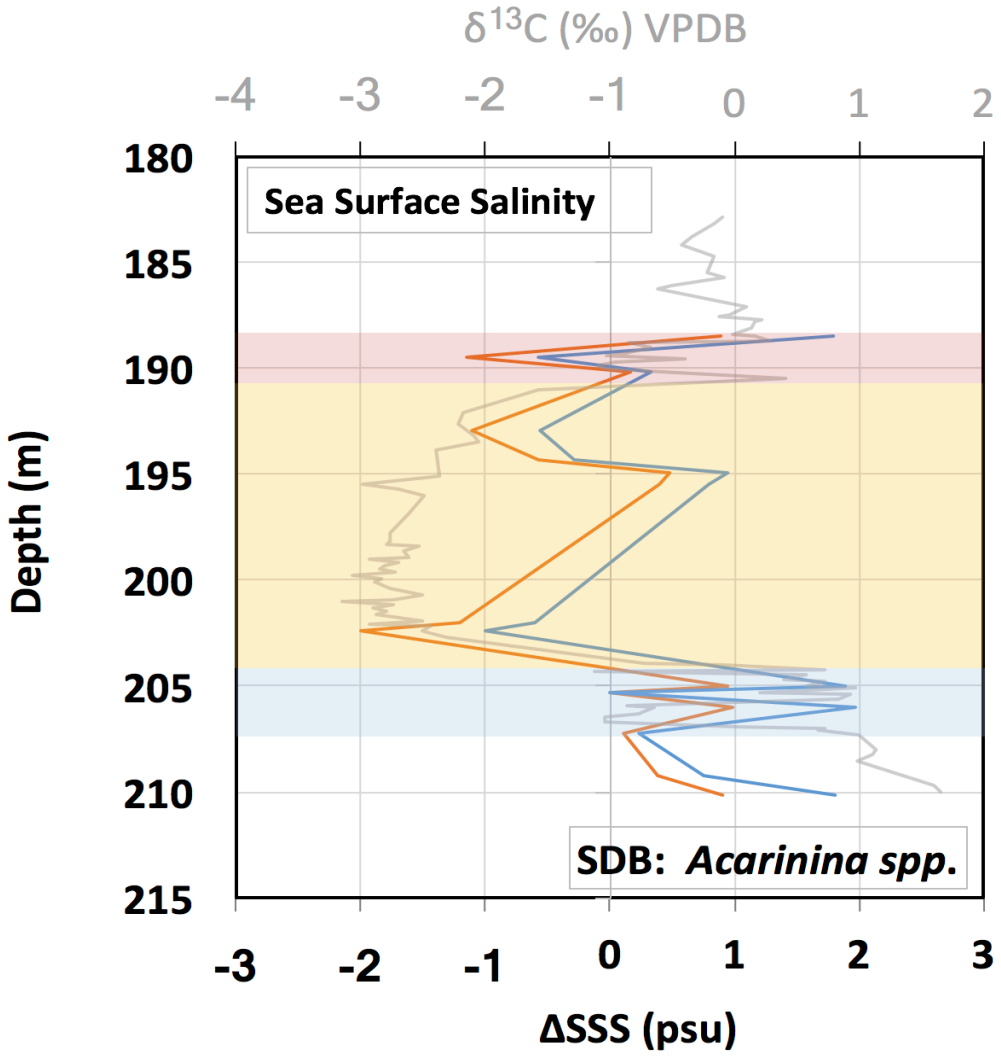

Figure 11: Relative changes in sea surface salinity based off coupled Mg/Ca and oxygen temperatures for foraminifera genera *Acarinina* spp. at site **SDB**. Base level salinities established at pre-CIE depth of 204 m. Also plotted are bulk $\delta^{13}C$ data for reference. Colors represent pre-CIE, CIE "core" and recovery intervals.

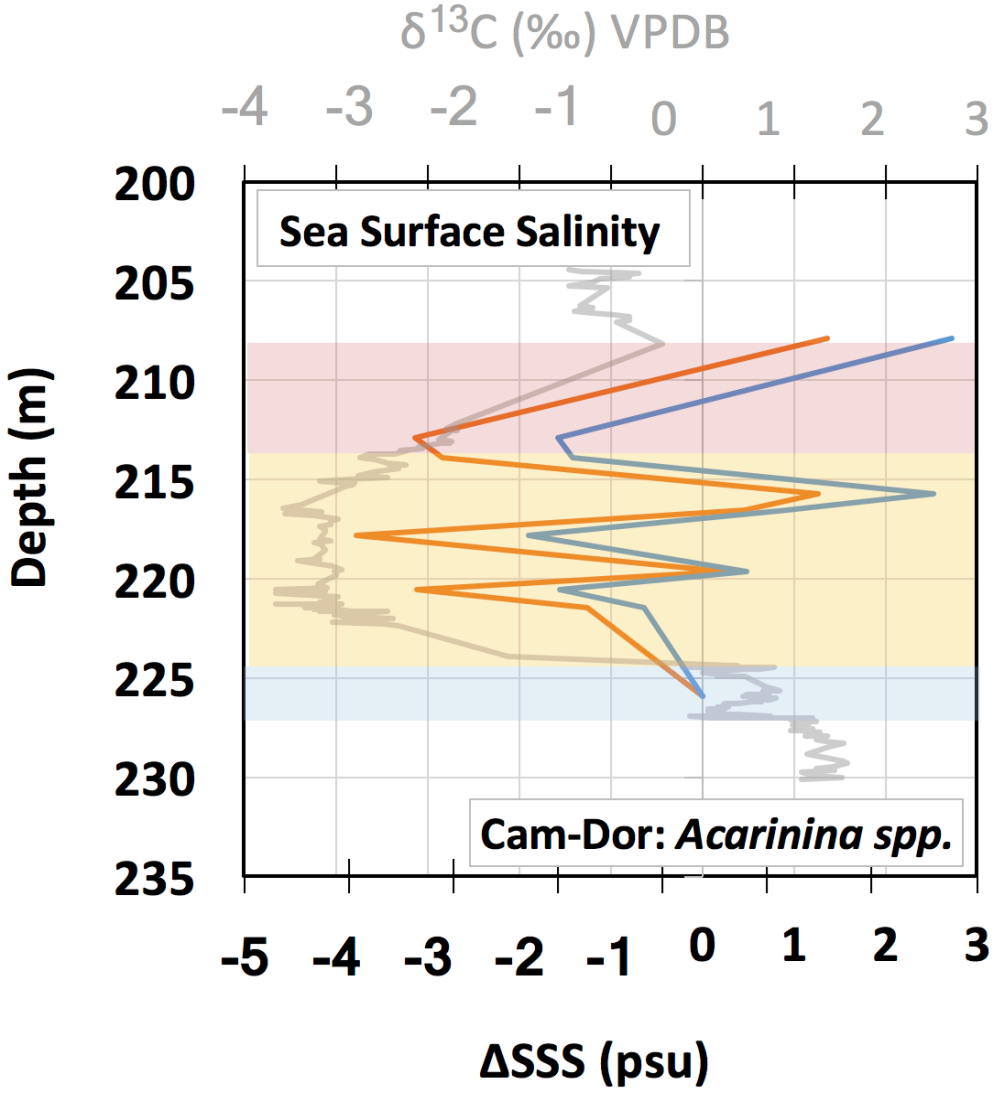

Figure 12: Relative changes in sea surface salinity based off coupled Mg/Ca and oxygen data for foraminifera genera *Acarinina* spp. at **Cam-Dor**. Base level salinities established at pre-CIE depth of 227 m. Also plotted are bulk $\delta^{13}C$ data for reference. Colors represent pre-CIE, CIE "core" and recovery intervals.

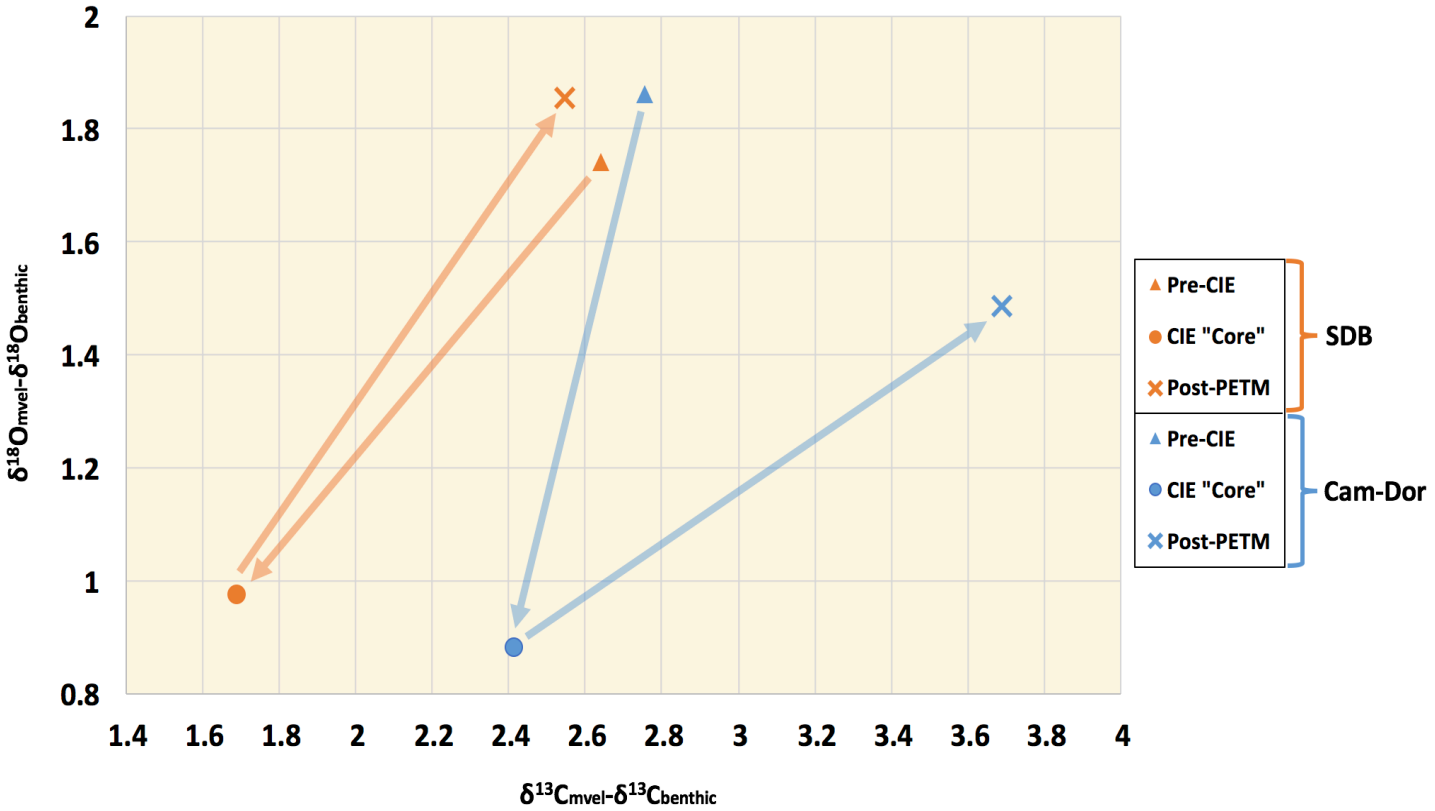

Figure 13: Cross plot of vertical $\delta^{13}C$ and $\delta^{18}O$ isotopic gradients. The range of vertical isotopic gradients are represented by the difference between the isotopic values of *Morozovella* spp. and benthic genera. Plotted are averages of isotopic values for sites SDB and Cam-Dor at pre-CIE, CIE "core" and post-PETM depth intervals.

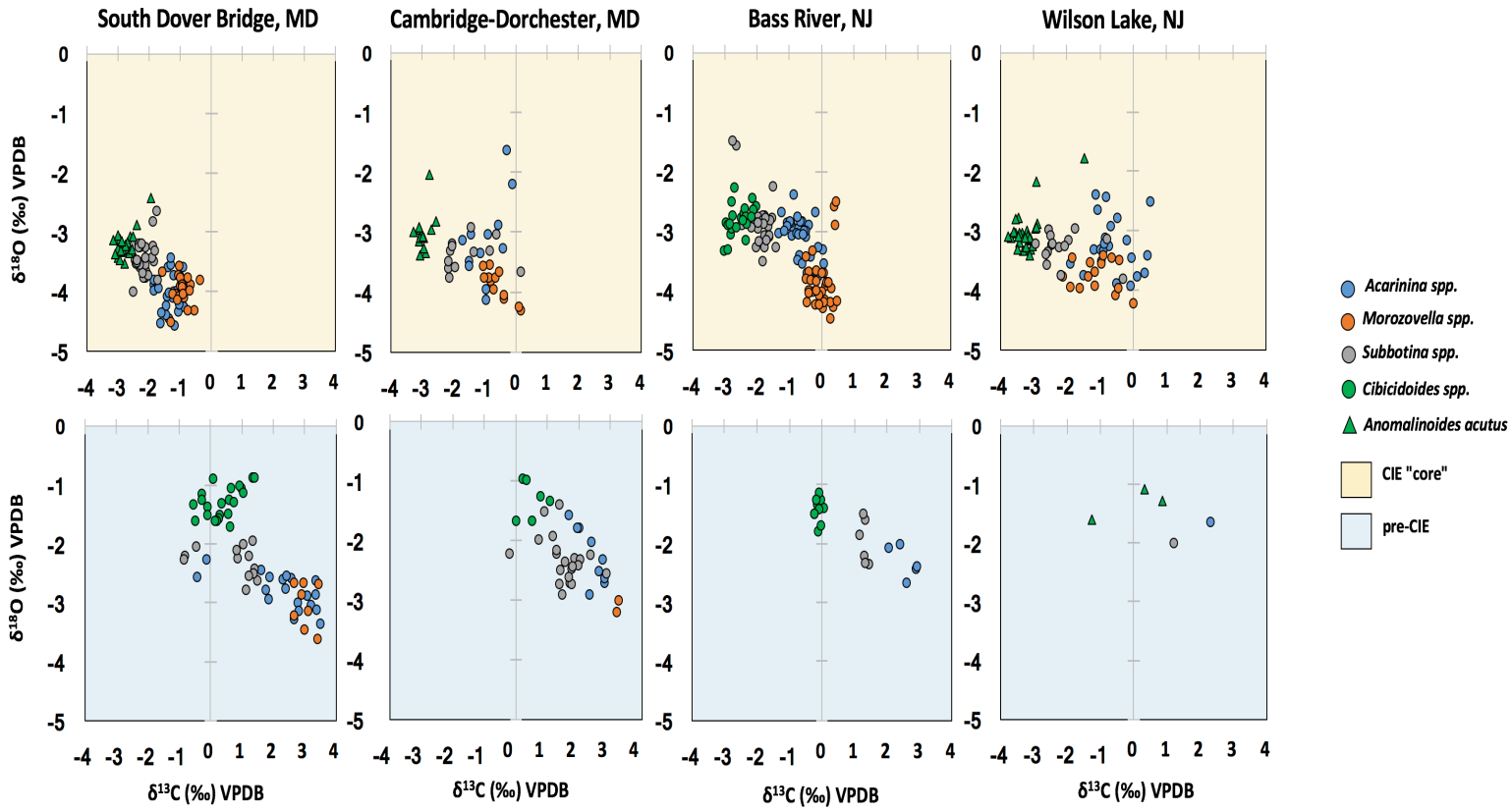

Figure 14: Cross plots of $\delta^{13}C$ and $\delta^{18}O$ isotopic data of mixed-layer, thermocline, and benthic foraminifera from South Dover Bridge, Cambridge-Dorchester, Bass River and Wilson Lake across the CIE onset. The lower panels represent pre-CIE and the upper, CIE intervals.

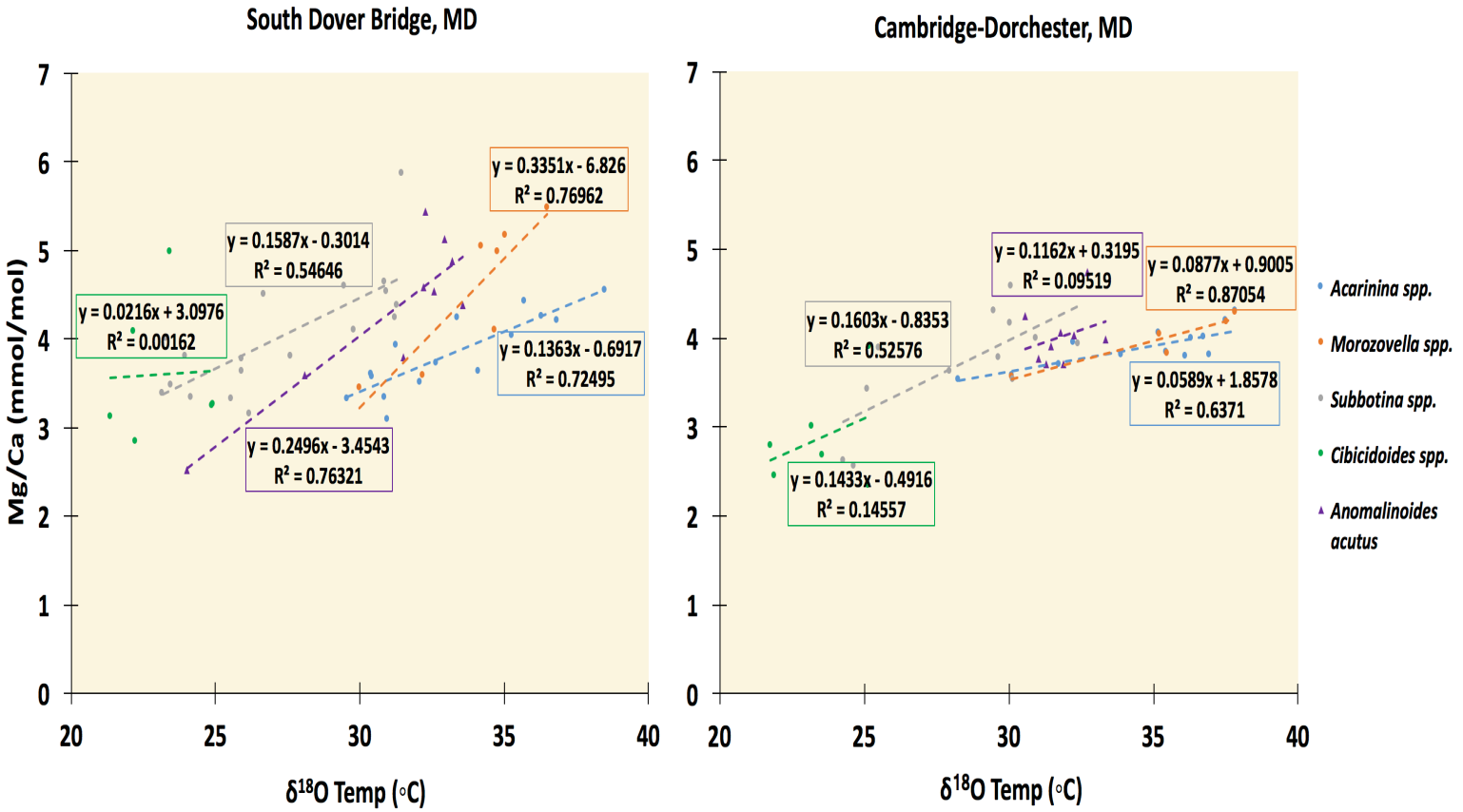

Figure 15: Mg/Ca plotted against $\delta^{18}O$ derived temperatures for South Dover Bridge and Cambridge-Dorchester. Linear regressions were used to fit data and generate calibration equations.

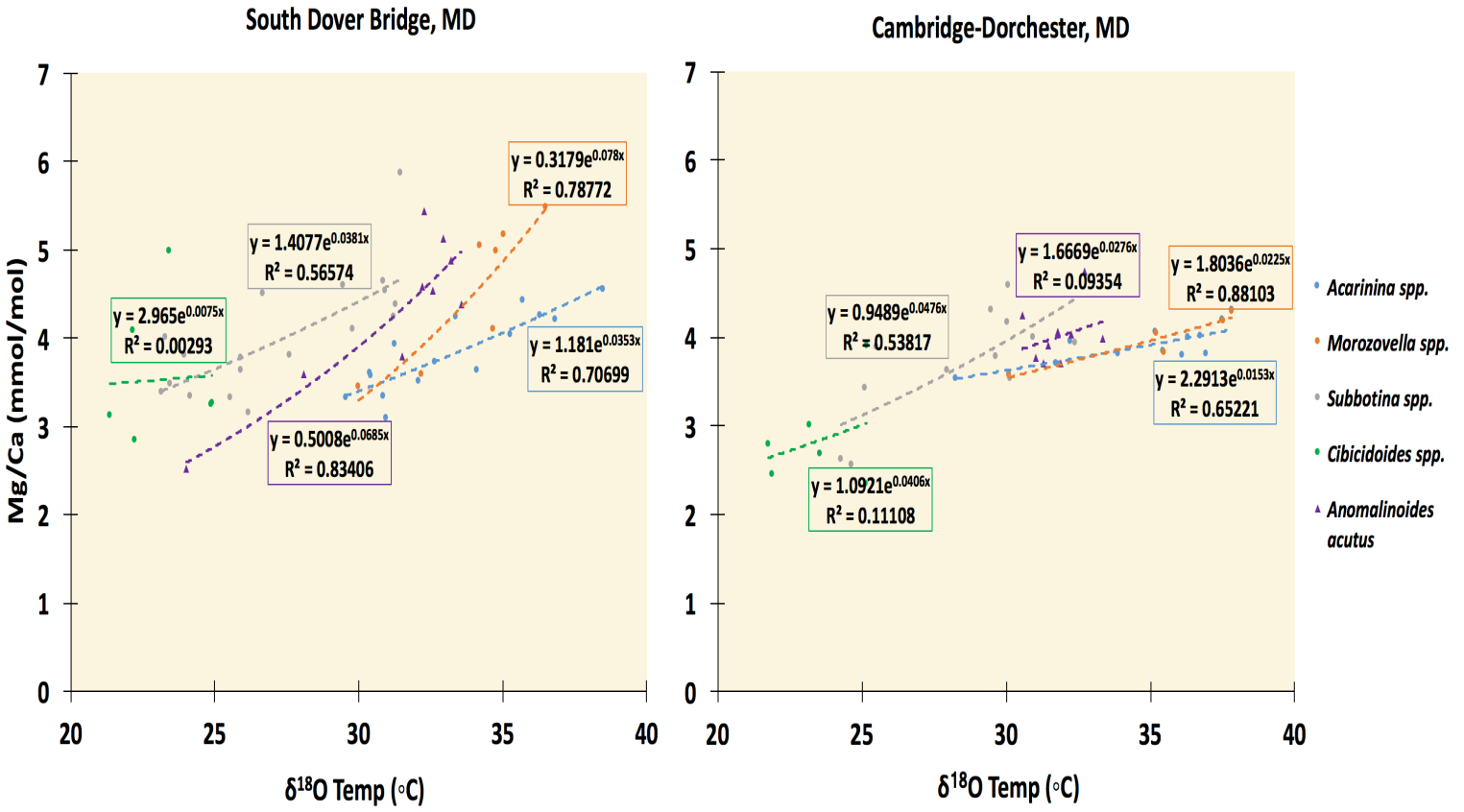

Figure 16: Foraminifera Mg/Ca plotted versus $\delta^{18}O$ derived temperatures for South Dover Bridge and Cambridge-Dorchester. Exponential regressions were used to fit data and generate calibration equations.

Data Tables

Site	Genera	Depth (ft)	Depth (m)	d13C	d18O		Site	Genera	Depth (ft)	Depth (m)	d13C	d18O
SDB	Acarinina	689.0	210.1	2.61	-2.60		SDB	Acarinina	652.0	198.9	-1.02	-4.10
SDB	Acarinina	688.0	209.8	3.37	-2.63		SDB	Acarinina	651.0	198.6	-1.84	-3.99
SDB	Acarinina	686.0	209.2	3.39	-2.87		SDB	Acarinina	650.1	198.3	-1.20	-3.74
SDB	Acarinina	685.0	208.9	2.81	-3.01		SDB	Acarinina	649.0	197.9	-1.69	-3.96
SDB	Acarinina	684.0	208.6	3.53	-3.36		SDB	Acarinina	648.0	197.6	-1.38	-3.59
SDB	Acarinina	683.0	208.3	3.23	-3.05		SDB	Acarinina	647.0	197.3	-1.27	-3.56
SDB	Acarinina	681.0	207.7	2.32	-2.62		SDB	Acarinina	646.4	197.2	-0.81	-3.94
SDB	Acarinina	679.5	207.2	3.43	-3.12		SDB	Acarinina	645.0	196.7	-1.00	-4.23
SDB	Acarinina	678.7	207.0	2.45	-2.55		SDB	Acarinina	643.0	196.1	-0.88	-3.59
SDB	Acarinina	678.0	206.8	-0.39	-2.57		SDB	Acarinina	642.0	195.8	-1.33	-4.04
SDB	Acarinina	677.3	206.6	-0.09	-2.27		SDB	Acarinina	641.4	195.6	-1.06	-4.00
SDB	Acarinina	675.0	205.9	1.88	-2.95		SDB	Acarinina	640.1	195.2	-1.28	-3.44
SDB	Acarinina	674.0	205.6	2.85	-3.15		SDB	Acarinina	639.0	194.9	-1.07	-3.39
SDB	Acarinina	673.0	205.3	3.11	-2.89		SDB	Acarinina	638.0	194.6	-0.57	-3.44
SDB	Acarinina	672.5	205.1	1.90	-2.58		SDB	Acarinina	637.0	194.3	-1.05	-3.88
SDB	Acarinina	672.0	205.0	2.41	-2.77		SDB	Acarinina	636.0	194.0	-0.94	-3.74
SDB	Acarinina	671.5	204.8	1.79	-2.79		SDB	Acarinina	635.0	193.7	-1.00	-3.15
SDB	Acarinina	670.9	204.6	1.64	-2.46		SDB	Acarinina	633.3	193.2	-1.07	-3.38
SDB	Acarinina	670.4	204.5	2.68	-3.30		SDB	Acarinina	632.0	192.8	-0.69	-3.79
SDB	Acarinina	664.5	202.7	-0.84	-4.28		SDB	Acarinina	631.0	192.5	-0.19	-3.97
SDB	Acarinina	664.0	202.5	-0.95	-4.13		SDB	Acarinina	630.1	192.2	-0.25	-3.81
SDB	Acarinina	663.5	202.4	-1.13	-4.11		SDB	Acarinina	626.0	190.9	-1.06	-2.91

SDB	Acarinina	663.0	202.2	-1.17	-4.57		SDB	Acarinina	626.0	190.9	0.02	-2.65
SDB	Acarinina	662.5	202.1	-1.33	-4.46		SDB	Acarinina	625.0	190.6	0.41	-3.32
SDB	Acarinina	662.0	201.9	-1.25	-4.10		SDB	Acarinina	623.4	190.1	0.46	-3.24
SDB	Acarinina	661.5	201.8	-1.62	-4.54		SDB	Acarinina	622.0	189.7	0.16	-3.44
SDB	Acarinina	661.0	201.6	-1.03	-4.35		SDB	Acarinina	621.5	189.6	0.51	-3.55
SDB	Acarinina	660.5	201.5	-1.43	-4.24		SDB	Acarinina	620.0	189.1	-0.02	-3.16
SDB	Acarinina	660.0	201.3	-1.21	-4.12		SDB	Acarinina	619.0	188.8	0.43	-2.66
SDB	Acarinina	659.5	201.1	-1.82	-3.89		SDB	Acarinina	618.5	188.6	1.55	-2.45
SDB	Acarinina	659.0	201.0	-1.39	-4.10		SDB	Acarinina	618.0	188.5	2.03	-2.78
SDB	Acarinina	658.0	200.7	-1.44	-4.40		SDB	Acarinina	617.5	188.3	2.12	-3.06
SDB	Acarinina	656.5	200.2	-1.20	-4.01		SDB	Acarinina	616.3	188.0	2.17	-3.02
SDB	Acarinina	655.6	200.0	-0.99	-3.75		SDB	Acarinina	610.5	186.2	-0.29	-3.29
SDB	Acarinina	654.6	199.7	-1.81	-3.81		SDB	Acarinina	610.5	186.2	1.29	-3.36
SDB	Acarinina	653.0	199.2	-1.57	-4.37		SDB	Acarinina	603.1	183.9	1.51	-3.31

Table 1

Site	Genera	Depth (ft)	Depth (m)	d13C	d18O		Site	Genera	Depth (ft)	Depth (m)	d13C	d18O
SDB	Morozvella	689.0	689.1	2.93	-2.86		SDB	Morozvella	655.0	655.1	-1.08	-4.16
SDB	Morozvella	686.0	686.1	3.45	-3.64		SDB	Morozvella	654.5	654.6	-0.34	-3.82
SDB	Morozvella	684.0	684.1	3.15	-3.15		SDB	Morozvella	653.5	653.6	-1.02	-3.57
SDB	Morozvella	679.5	679.6	3.00	-2.68		SDB	Morozvella	652.0	652.1	-0.96	-3.90
SDB	Morozvella	678.4	678.5	2.70	-2.67		SDB	Morozvella	651.0	651.1	-0.52	-4.33
SDB	Morozvella	675.0	675.1	2.69	-3.22		SDB	Morozvella	650.5	650.6	-0.93	-3.90
SDB	Morozvella	673.0	673.1	3.46	-2.69		SDB	Morozvella	647.0	647.1	-0.92	-3.93
SDB	Morozvella	670.4	670.5	3.03	-3.47		SDB	Morozvella	646.1	646.2	-0.87	-4.05
SDB	Morozvella	664.0	664.1	-1.14	-4.05		SDB	Morozvella	645.0	645.1	-0.72	-4.33
SDB	Morozvella	663.0	663.1	-0.86	-4.11		SDB	Morozvella	642.0	642.1	-0.66	-3.99
SDB	Morozvella	662.5	662.6	-1.03	-3.74		SDB	Morozvella	641.4	641.5	-0.73	-3.77
SDB	Morozvella	661.0	661.1	-1.23	-4.06		SDB	Morozvella	636.0	636.1	-0.41	-3.86
SDB	Morozvella	660.5	660.6	-0.63	-3.90		SDB	Morozvella	633.3	633.4	-0.15	-4.31
SDB	Morozvella	659.5	659.6	-1.29	-4.52		SDB	Morozvella	626.0	626.1	0.78	-3.35
SDB	Morozvella	658.5	658.6	-0.97	-3.78		SDB	Morozvella	619.0	619.1	1.32	-3.58
SDB	Morozvella	657.0	657.1	-0.99	-4.09		SDB	Morozvella	617.5	617.6	2.43	-3.67
SDB	Morozvella	656.0	656.1	-1.55	-3.69		SDB	Morozvella	609.1	609.2	1.67	-3.10

Table 2

Site	Genera	Depth (ft)	Depth (m)	d13C	d18O		Site	Genera	Depth (ft)	Depth (m)	d13C	d18O
SDB	Subbotina	689.0	210.1	1.36	-1.97		SDB	Subbotina	651.5	198.7	-2.29	-3.26
SDB	Subbotina	686.0	209.2	1.42	-2.43		SDB	Subbotina	651.0	198.6	-2.40	-3.54
SDB	Subbotina	685.0	208.9	1.25	-2.21		SDB	Subbotina	650.5	198.4	-2.36	-3.52
SDB	Subbotina	684.0	208.6	1.53	-2.64		SDB	Subbotina	650.1	198.3	-2.36	-3.48
SDB	Subbotina	679.5	207.2	1.39	-2.51		SDB	Subbotina	649.0	197.9	-2.67	-3.28
SDB	Subbotina	678.7	207.0	0.89	-2.25		SDB	Subbotina	647.0	197.3	-1.85	-3.25
SDB	Subbotina	678.0	206.8	-0.42	-2.06		SDB	Subbotina	646.1	197.1	-2.33	-3.27
SDB	Subbotina	677.5	206.6	-0.80	-2.23		SDB	Subbotina	645.0	196.7	-2.22	-3.21
SDB	Subbotina	676.5	206.3	-0.82	-2.28		SDB	Subbotina	644.0	196.4	-1.70	-3.82
SDB	Subbotina	675.0	205.9	0.87	-2.12		SDB	Subbotina	643.0	196.1	-1.89	-3.44
SDB	Subbotina	674.0	205.6	1.16	-2.79		SDB	Subbotina	641.4	195.6	-2.11	-3.44
SDB	Subbotina	673.0	205.3	1.25	-2.56		SDB	Subbotina	640.1	195.2	-1.80	-3.32
SDB	Subbotina	671.5	204.8	1.08	-2.02		SDB	Subbotina	639.0	194.9	-1.81	-2.99
SDB	Subbotina	663.5	202.4	-2.13	-3.48		SDB	Subbotina	638.0	194.6	-1.84	-3.33
SDB	Subbotina	663.0	202.2	-2.28	-3.60		SDB	Subbotina	637.0	194.3	-1.83	-3.45
SDB	Subbotina	662.5	202.1	-1.84	-3.50		SDB	Subbotina	636.0	194.0	-1.50	-3.05
SDB	Subbotina	662.0	201.9	-2.11	-3.79		SDB	Subbotina	635.0	193.7	-2.10	-3.25
SDB	Subbotina	661.5	201.8	-1.86	-2.84		SDB	Subbotina	633.3	193.2	-2.02	-3.28
SDB	Subbotina	660.5	201.5	-2.10	-3.64		SDB	Subbotina	632.0	192.8	-1.95	-3.27
SDB	Subbotina	659.0	201.0	-1.75	-2.66		SDB	Subbotina	631.0	192.5	-1.60	-3.28
SDB	Subbotina	658.0	200.7	-2.48	-3.22		SDB	Subbotina	630.1	192.2	-1.74	-3.39
SDB	Subbotina	657.0	200.4	-2.15	-3.78		SDB	Subbotina	626.8	191.2	-0.72	-2.39

SDB	Subbotina	656.5	200.2	-2.32	-3.21		SDB	Subbotina	623.4	190.1	-1.04	-2.84
SDB	Subbotina	656.0	200.1	-2.06	-3.68		SDB	Subbotina	622.0	189.7	-0.66	-2.64
SDB	Subbotina	655.6	200.0	-2.38	-3.49		SDB	Subbotina	619.3	188.9	0.32	-1.74
SDB	Subbotina	655.0	199.8	-2.50	-4.02		SDB	Subbotina	618.5	188.6	0.11	-2.16
SDB	Subbotina	654.5	199.6	-2.44	-3.48		SDB	Subbotina	617.5	188.3	0.36	-2.02
SDB	Subbotina	654.0	199.5	-2.09	-3.26		SDB	Subbotina	616.3	188.0	0.02	-1.99
SDB	Subbotina	653.5	199.3	-2.02	-3.73		SDB	Subbotina	611.1	186.4	-0.86	-3.16
SDB	Subbotina	653.0	199.2	-2.11	-3.56		SDB	Subbotina	609.1	185.8	-0.09	-2.51
SDB	Subbotina	652.5	199.0	-2.20	-3.69		SDB	Subbotina	602.1	183.6	0.86	-2.76
SDB	Subbotina	652.0	198.9	-2.27	-3.57							

Table 3

Site	Genera	Depth (ft)	Depth (m)	d13C corr	d18O corr		Site	Genera	Depth (ft)	Depth (m)	d13C corr	d18O corr
SDB	Cibicidoides	684.2	208.7	1.01	-1.07		SDB*	A. acutus	661.6	201.8	-2.56	-3.29
SDB	Cibicidoides	683.2	208.4	0.61	-1.26		SDB*	A. acutus	661.6	201.8	-2.81	-3.53
SDB	Cibicidoides	682.7	208.2	1.37	-0.89		SDB*	A. acutus	661.2	201.7	-2.85	-3.29
SDB	Cibicidoides	681.2	207.8	0.96	-1.02		SDB*	A. acutus	660.7	201.5	-2.96	-3.11
SDB	Cibicidoides	680.2	207.5	0.69	-1.06		SDB*	A. acutus	660.2	201.4	-1.94	-2.43
SDB	Cibicidoides	679.7	207.3	0.77	-1.30		SDB*	A. acutus	659.5	201.2	-2.95	-3.46
SDB	Cibicidoides	679.6	207.3	-0.07	-1.39		SDB*	A. acutus	659.2	201.0	-2.63	-3.06
SDB	Cibicidoides	679.2	207.1	1.06	-1.14		SDB*	A. acutus	658.7	200.9	-3.15	-3.14
SDB	Cibicidoides	678.7	207.0	1.44	-0.88		SDB*	A. acutus	657.5	200.5	-2.71	-3.17
SDB	Cibicidoides	678.2	206.9	-0.52	-1.34		SDB*	A. acutus	657.2	200.4	-3.01	-3.05
SDB	Cibicidoides	677.2	206.5	0.12	-0.90		SDB*	A. acutus	655.1	199.8	-2.75	-3.23

SDB	Cibicidoides	676.7	206.4	-0.25	-1.17		SDB*	A. acutus	653.1	199.2	-3.10	-3.36
SDB	Cibicidoides	676.2	206.2	-0.24	-1.27		SDB*	A. acutus	650.6	198.4	-2.88	-3.15
SDB	Cibicidoides	675.7	206.1	-0.47	-1.63		SDB*	A. acutus	647.1	197.4	-2.93	-3.30
SDB	Cibicidoides	675.2	205.9	0.32	-1.52		SDB*	A. acutus	644.1	196.5	-2.41	-2.86
SDB	Cibicidoides	674.7	205.8	0.30	-1.58		SDB*	A. acutus	640.2	195.3	-2.53	-3.08
SDB	Cibicidoides	674.2	205.6	0.38	-1.32		SDB*	A. acutus	636.1	194.0	-2.08	-2.68
SDB	Cibicidoides	673.7	205.5	0.66	-1.73		SDB*	A. acutus	632.1	192.8	-2.27	-3.00
SDB	Cibicidoides	672.7	205.2	0.24	-1.63		SDB*	A. acutus	631.1	192.5	-1.69	-3.01
SDB	Cibicidoides	672.1	205.0	-0.06	-1.53		SDB*	A. acutus	626.1	191.0	-1.60	-1.65
SDB	Cibicidoides	670.7	204.6	0.59	-1.50		SDB*	A. acutus	623.5	190.2	-1.10	-2.29
SDB	Cibicidoides	670.2	204.4	0.17	-1.62		SDB*	A. acutus	621.1	189.4	-1.74	-1.80
SDB	A. acutus	664.7	202.7	-2.78	-3.21		SDB*	A. acutus	619.6	189.0	-0.63	-1.48
SDB	A. acutus	664.1	202.6	-2.87	-3.33		SDB*	A. acutus	617.1	188.2	-0.40	-1.55

SDB	A. acutus	663.2	202.3	-3.00	-3.26		SDB*	A. acutus	615.6	187.8	-0.36	-1.45
SDB*	A. acutus	662.7	202.1	-2.65	-3.34		SDB*	A. acutus	613.8	187.2	-0.73	-1.60
SDB*	A. acutus	662.0	201.9	-3.02	-3.43							

Table 4

Site	Genera	Depth (ft)	Depth (m)	Line	d13C uncorr	d18O uncorr	d13C dup	d18O dup	d13C diff	d18O diff
SDB*	A. acutus	655.1	199.8	1	-3.13	-3.66	-3.05	-3.39	0.07	0.27
SDB*	A. acutus	653.1	199.2	2	-2.70	-2.86	-3.32	-3.33	0.62	0.48
SDB*	A. acutus	647.1	197.4	2	-2.53	-2.80	-2.76	-3.12	0.23	0.32
SDB*	A. acutus	644.1	196.5	1	-2.78	-3.30	-2.59	-2.99	0.20	0.31
SDB*	A. acutus	640.2	195.3	2	-2.13	-2.58	-2.39	-3.03	0.26	0.45
SDB*	A. acutus	626.1	191.0	2	-1.19	-1.15	-1.78	-1.91	0.59	0.76
SDB*	A. acutus	619.6	189.0	1	-1.00	-1.91	-0.15	-1.20	0.86	0.71

Table 5

Site	Genera	Depth (ft)	Depth (m)	d13C uncorr	d18O uncorr
SDB*	A. acutus	662.7	202.1	-3.02	-3.77
SDB*	A. acutus	662.0	201.9	-2.62	-2.93
SDB*	A. acutus	661.6	201.8	-2.93	-3.72
SDB*	A. acutus	661.6	201.8	-2.41	-3.03
SDB*	A. acutus	661.2	201.7	-3.22	-3.72
SDB*	A. acutus	660.7	201.5	-2.56	-2.61
SDB*	A. acutus	660.2	201.4	-2.31	-2.86
SDB*	A. acutus	659.5	201.2	-2.55	-2.96
SDB*	A. acutus	659.2	201.0	-3.01	-3.49
SDB*	A. acutus	658.7	200.9	-2.75	-2.64
SDB*	A. acutus	657.5	200.5	-3.08	-3.60
SDB*	A. acutus	657.2	200.4	-2.61	-2.55
SDB*	A. acutus	655.1	199.8	-3.13	-3.66
SDB*	A. acutus	653.1	199.2	-2.70	-2.86
SDB*	A. acutus	650.6	198.4	-3.25	-3.58
SDB*	A. acutus	647.1	197.4	-2.53	-2.80
SDB*	A. acutus	644.1	196.5	-2.78	-3.30
SDB*	A. acutus	640.2	195.3	-2.13	-2.58
SDB*	A. acutus	636.1	194.0	-2.46	-3.11
SDB*	A. acutus	632.1	192.8	-1.86	-2.50
SDB*	A. acutus	631.1	192.5	-2.06	-3.44
SDB*	A. acutus	626.1	191.0	-1.19	-1.15
SDB*	A. acutus	623.5	190.2	-1.48	-2.72
SDB*	A. acutus	621.1	189.4	-1.34	-1.30
SDB*	A. acutus	619.6	189.0	-1.00	-1.91

SDB*	A. acutus	617.1	188.2	0.00	-1.04
SDB*	A. acutus	615.6	187.8	-0.74	-1.88
SDB*	A. acutus	613.8	187.2	-0.33	-1.10

Table 6

Site	Genera	Depth (ft)	Depth (m)	Mg/Ca		Site	Genera	Depth (ft)	Depth (m)	Mg/Ca
SDB	Acarinina	689.1	210.2	3.33		SDB	Morozovella	653.8	199.4	5.05
SDB	Acarinina	686.1	209.2	3.34		SDB	Morozovella	639.1	194.9	5.07
SDB	Acarinina	679.6	207.3	3.51		SDB	Morozovella	617.8	188.4	4.10
SDB	Acarinina	675.3	206.0	3.93		SDB	Subbotina	688.6	210.0	3.38
SDB	Acarinina	673.1	205.3	3.10		SDB	Subbotina	686.1	209.2	3.32
SDB	Acarinina	672.1	205.0	3.60		SDB	Subbotina	679.6	207.3	3.77
SDB	Acarinina	663.6	202.4	4.22		SDB	Subbotina	675.3	206.0	3.80
SDB	Acarinina	662.3	202.0	4.55		SDB	Subbotina	673.1	205.3	3.16
SDB	Acarinina	640.8	195.4	4.26		SDB	Subbotina	671.4	204.8	3.48
SDB	Acarinina	639.1	194.9	4.25		SDB	Subbotina	662.8	202.2	5.87
SDB	Acarinina	637.1	194.3	4.44		SDB	Subbotina	659.8	201.2	4.49
SDB	Acarinina	632.6	192.9	4.04		SDB	Subbotina	655.8	200.0	4.53
SDB	Acarinina	628.1	191.6	4.16		SDB	Subbotina	654.3	199.6	4.64
SDB	Acarinina	623.5	190.2	3.73		SDB	Subbotina	653.3	199.3	4.24
SDB	Acarinina	621.3	189.5	3.63		SDB	Subbotina	652.3	199.0	4.37
SDB	Acarinina	618.1	188.5	3.58		SDB	Subbotina	645.6	196.9	4.59
SDB	Acarinina	613.8	187.2	3.71		SDB	Subbotina	631.8	192.7	4.09
SDB	Acarinina	599.2	182.8	4.35		SDB	Subbotina	624.5	190.5	3.80
SDB	Morozovella	684.3	208.7	3.58		SDB	Subbotina	618.8	188.7	3.34
SDB	Morozovella	673.1	205.3	3.44		SDB	Subbotina	615.7	187.8	4.00
SDB	Morozovella	663.6	202.4	5.48		SDB	Subbotina	609.9	186.0	3.63
SDB	Morozovella	662.3	202.0	5.17		SDB	Subbotina	599.2	182.8	3.66
SDB	Morozovella	656.2	200.1	4.98						

Table 7

Site	Genera	Depth (ft)	Depth (m)	Mg/Ca
SDB	A.acutus	616.0	187.9	2.52
SDB	A.acutus	618.5	188.6	3.23
SDB	A.acutus	623.4	190.1	3.59
SDB	A.acutus	630.1	192.2	3.80
SDB	A.acutus	634.0	193.4	3.67
SDB	A.acutus	635.0	193.7	3.81
SDB	A.acutus	638.0	194.6	4.06
SDB	A.acutus	646.1	197.1	5.13
SDB	A.acutus	649.0	197.9	5.36
SDB	A.acutus	651.0	198.6	4.59
SDB	A.acutus	653.5	199.3	4.88
SDB	A.acutus	655.6	200.0	4.55
SDB	A.acutus	657.5	200.5	5.43
SDB	A.acutus	662.0	201.9	4.38
SDB	Cibicidoides	670.0	204.4	3.26
SDB	Cibicidoides	673.0	205.3	3.26
SDB	Cibicidoides	674.0	205.6	4.99
SDB	Cibicidoides	680.0	207.4	4.09
SDB	Cibicidoides	682.0	208.0	3.13
SDB	Cibicidoides	684.0	208.6	2.85
SDB	Cibicidoides	688.0	209.8	3.65

Table 8

Site	Genera	Depth (ft)	Depth (m)	d13C	d18O
Cam-Dor	Acarinina	751.0	229.1	2.43	-2.04
Cam-Dor	Acarinina	749.1	228.5	2.77	-2.33
Cam-Dor	Acarinina	747.1	227.9	1.69	-1.57
Cam-Dor	Acarinina	743.1	226.6	2.03	-1.79
Cam-Dor	Acarinina	739.7	225.6	2.36	-2.92
Cam-Dor	Acarinina	738.5	225.2	1.98	-1.79
Cam-Dor	Acarinina	737.5	224.9	2.65	-2.53
Cam-Dor	Acarinina	736.8	224.7	2.83	-2.73
Cam-Dor	Acarinina	735.9	224.5	2.84	-2.64
Cam-Dor	Acarinina	727.2	221.8	-0.40	-3.28
Cam-Dor	Acarinina	725.3	221.2	-1.49	-3.50
Cam-Dor	Acarinina	723.3	220.6	-0.94	-3.96
Cam-Dor	Acarinina	721.1	219.9	-1.68	-3.16
Cam-Dor	Acarinina	719.3	219.4	-0.27	-1.65
Cam-Dor	Acarinina	717.4	218.8	-1.47	-3.58
Cam-Dor	Acarinina	715.1	218.1	-1.11	-3.36
Cam-Dor	Acarinina	713.2	217.5	-0.92	-4.14
Cam-Dor	Acarinina	711.1	216.9	-1.41	-3.06
Cam-Dor	Acarinina	709.2	216.3	-0.55	-2.89
Cam-Dor	Acarinina	707.4	215.7	-0.10	-2.22
Cam-Dor	Acarinina	705.2	215.1	-0.89	-3.05
Cam-Dor	Acarinina	703.1	214.4	-0.25	-3.19
Cam-Dor	Acarinina	701.3	213.9	-0.69	-4.01
Cam-Dor	Acarinina	698.9	213.1	-0.07	-3.39
Cam-Dor	Acarinina	697.1	212.6	0.12	-4.10
Cam-Dor	Acarinina	682.1	208.0	4.03	-2.33

Table 9

Site	Genera	Depth (ft)	Depth (m)	d13C	d18O
Cam-Dor	Morozovella	737.5	224.9	3.23	-3.21
Cam-Dor	Morozovella	736.3	224.6	3.30	-3.02
Cam-Dor	Morozovella	727.2	221.8	-0.78	-3.83
Cam-Dor	Morozovella	725.3	221.2	-0.80	-3.55
Cam-Dor	Morozovella	723.3	220.6	0.18	-4.32
Cam-Dor	Morozovella	721.1	219.9	-0.83	-3.77
Cam-Dor	Morozovella	719.3	219.4	-0.35	-4.12
Cam-Dor	Morozovella	717.4	218.8	-0.63	-3.77
Cam-Dor	Morozovella	715.1	218.1	-1.01	-3.77
Cam-Dor	Morozovella	713.2	217.5	0.12	-4.26
Cam-Dor	Morozovella	711.1	216.9	-1.01	-3.58
Cam-Dor	Morozovella	709.2	216.3	-0.69	-3.97
Cam-Dor	Morozovella	707.4	215.7	-0.36	-4.06
Cam-Dor	Morozovella	705.2	215.1	-0.50	-3.67
Cam-Dor	Morozovella	703.1	214.4	0.94	-4.01
Cam-Dor	Morozovella	698.9	213.1	1.56	-4.22
Cam-Dor	Morozovella	682.1	208.0	3.14	-2.72

Table 10

Site	Genera	Depth (ft)	Depth (m)	d13C	d18O
Cam-Dor	Subbotina	751.0	229.1	1.72	-2.73
Cam-Dor	Subbotina	749.1	228.5	2.91	-2.57
Cam-Dor	Subbotina	745.3	227.3	1.89	-2.30
Cam-Dor	Subbotina	745.1	227.2	1.79	-2.48
Cam-Dor	Subbotina	743.1	226.6	1.43	-2.51
Cam-Dor	Subbotina	741.1	226.0	1.31	-2.23
Cam-Dor	Subbotina	740.3	225.8	2.39	-2.25
Cam-Dor	Subbotina	739.9	225.7	2.06	-2.32
Cam-Dor	Subbotina	739.7	225.6	2.01	-2.43
Cam-Dor	Subbotina	739.3	225.5	1.40	-1.41
Cam-Dor	Subbotina	738.5	225.2	0.75	-2.00
Cam-Dor	Subbotina	738.3	225.2	1.78	-2.75
Cam-Dor	Subbotina	738.0	225.1	1.58	-2.37
Cam-Dor	Subbotina	737.8	225.0	1.70	-2.63
Cam-Dor	Subbotina	737.5	224.9	1.82	-2.45
Cam-Dor	Subbotina	736.8	224.7	0.93	-1.53
Cam-Dor	Subbotina	736.3	224.6	1.33	-2.18
Cam-Dor	Subbotina	736.1	224.5	1.50	-2.91
Cam-Dor	Subbotina	735.9	224.5	1.19	-1.93
Cam-Dor	Subbotina	735.5	224.3	1.40	-2.75
Cam-Dor	Subbotina	735.3	224.3	-0.19	-2.23
Cam-Dor	Subbotina	727.2	221.8	-2.14	-3.61
Cam-Dor	Subbotina	725.3	221.2	-2.15	-3.50
Cam-Dor	Subbotina	723.3	220.6	-1.93	-3.60
Cam-Dor	Subbotina	721.1	219.9	-2.01	-3.20
Cam-Dor	Subbotina	719.3	219.4	-0.61	-3.06
Cam-Dor	Subbotina	717.4	218.8	-2.06	-3.32

Cam-Dor	Subbotina	715.1	218.1	-2.09	-3.78
Cam-Dor	Subbotina	713.2	217.5	-2.01	-3.24
Cam-Dor	Subbotina	709.2	216.3	0.19	-3.68
Cam-Dor	Subbotina	711.1	216.9	-1.41	-2.93
Cam-Dor	Subbotina	707.4	215.7	-0.82	-3.32
Cam-Dor	Subbotina	705.2	215.1	-1.33	-3.34
Cam-Dor	Subbotina	703.1	214.4	-1.83	-2.91
Cam-Dor	Subbotina	697.1	212.6	-1.03	-2.42
Cam-Dor	Subbotina	682.1	208.0	0.85	-2.34

Table 11

Site	Genera	Depth (ft)	Depth (m)	d13C	d18O
Cam-Dor	Cibicidoides	749.1	228.5	1.10	-1.35
Cam-Dor	Cibicidoides	745.1	227.2	0.79	-1.27
Cam-Dor	Cibicidoides	743.1	226.6	0.03	-1.68
Cam-Dor	Cibicidoides	741.1	226.0	0.23	-0.97
Cam-Dor	Cibicidoides	739.2	225.4	0.37	-1.00
Cam-Dor	Cibicidoides	737.2	224.8	0.53	-1.68
Cam-Dor	A. acutus	735.2	224.2	-2.78	-2.04
Cam-Dor	A. acutus	729.0	222.3	-2.88	-3.34
Cam-Dor	A. acutus	727.2	221.8	-3.07	-3.39
Cam-Dor	A. acutus	725.3	221.2	-2.93	-3.26
Cam-Dor	A. acutus	723.3	220.6	-3.11	-3.16
Cam-Dor	A. acutus	721.1	219.9	-3.07	-2.96
Cam-Dor	A. acutus	719.3	219.4	-3.04	-3.03
Cam-Dor	A. acutus	717.4	218.8	-3.07	-3.09
Cam-Dor	A. acutus	715.1	218.1	-2.94	-3.09
Cam-Dor	A. acutus	713.2	217.5	-2.99	-3.07
Cam-Dor	A. acutus	711.1	216.9	-3.28	-3.00
Cam-Dor	A. acutus	709.2	216.3	-3.09	-2.91
Cam-Dor	A. acutus	707.4	215.7	-2.57	-2.81
Cam-Dor	A. acutus	705.2	215.1	-2.72	-2.96
Cam-Dor	A. acutus	703.1	214.4	-2.05	-2.59
Cam-Dor	A. acutus	701.3	213.9	-2.33	-2.43
Cam-Dor	A. acutus	698.9	213.1	-1.83	-2.34
Cam-Dor	A. acutus	697.1	212.6	-1.86	-2.35
Cam-Dor	A. acutus	682.1	208.0	-0.55	-1.23

Table 12

Site	Genera	Depth (ft)	Depth (m)	Mg/Ca		Site	Genera	Depth (ft)	Depth (m)	Mg/Ca
Cam-Dor	Acarinina	740.6	225.9	3.40		Cam-Dor	Morozovella	701.3	213.9	4.11
Cam-Dor	Acarinina	729.0	222.3	3.30		Cam-Dor	Morozovella	698.0	212.9	3.96
Cam-Dor	Acarinina	726.2	221.5	3.81		Cam-Dor	Morozovella	681.7	207.9	3.58
Cam-Dor	Acarinina	723.3	220.6	3.80		Cam-Dor	Subbotina	740.6	225.9	2.57
Cam-Dor	Acarinina	720.2	219.6	3.95		Cam-Dor	Subbotina	736.2	224.5	2.63
Cam-Dor	Acarinina	714.1	217.8	3.81		Cam-Dor	Subbotina	729.0	222.3	3.77
Cam-Dor	Acarinina	710.1	216.6	3.71		Cam-Dor	Subbotina	726.2	221.5	4.00
Cam-Dor	Acarinina	707.4	215.7	4.39		Cam-Dor	Subbotina	720.2	219.6	4.31
Cam-Dor	Acarinina	704.1	214.8	4.05		Cam-Dor	Subbotina	717.4	218.8	4.59
Cam-Dor	Acarinina	701.3	213.9	3.99		Cam-Dor	Subbotina	715.1	218.1	3.94
Cam-Dor	Acarinina	698.0	212.9	4.01		Cam-Dor	Subbotina	713.2	217.5	3.79
Cam-Dor	Acarinina	681.7	207.9	3.53		Cam-Dor	Subbotina	707.4	215.7	4.17
Cam-Dor	Morozovella	727.2	221.8	3.83		Cam-Dor	Subbotina	705.2	215.1	3.54
Cam-Dor	Morozovella	724.3	220.9	4.30		Cam-Dor	Subbotina	702.2	214.2	3.63
Cam-Dor	Morozovella	717.4	218.8	4.05		Cam-Dor	Subbotina	698.0	212.9	3.89
Cam-Dor	Morozovella	713.2	217.5	4.19		Cam-Dor	Subbotina	681.7	207.9	3.43
Cam-Dor	Morozovella	704.1	214.8	4.21						

Table 13

Site	Genera	Depth (ft)	Depth (m)	Mg/Ca
Cam-Dor	Cibicidoides	750.1	228.8	2.69
Cam-Dor	Cibicidoides	747.0	227.8	3.00
Cam-Dor	Cibicidoides	745.2	227.3	3.02
Cam-Dor	Cibicidoides	743.6	226.8	3.91
Cam-Dor	Cibicidoides	741.6	226.2	2.79
Cam-Dor	Cibicidoides	739.2	225.4	2.46
Cam-Dor	Cibicidoides	737.2	224.8	2.34
Cam-Dor	A. acutus	727.2	221.8	3.98
Cam-Dor	A. acutus	725.3	221.2	4.74
Cam-Dor	A. acutus	723.3	220.6	4.03
Cam-Dor	A. acutus	720.2	219.6	3.70
Cam-Dor	A. acutus	717.4	218.8	3.71
Cam-Dor	A. acutus	714.1	217.8	4.06
Cam-Dor	A. acutus	711.1	216.9	3.92
Cam-Dor	A. acutus	709.2	216.3	3.77
Cam-Dor	A. acutus	707.4	215.7	4.24
Cam-Dor	A. acutus	704.1	214.8	3.83
Cam-Dor	A. acutus	698.0	212.9	3.48

Table 14

Standard	Weight (ug)	d13C	d18O		Standard	Weight (ug)	d13C	d18O
CM12	27	2.06	-1.92		CM12	22	1.84	-2.31
CM12	34	2.02	-1.87		CM12	9	1.86	-2.15
CM12	16	1.72	-1.38		CM12	18	1.94	-2.13
CM12	21	2.11	-1.87		CM12	17	2.04	-1.88
CM12	19	1.99	-1.94		CM12	16	2.08	-1.81
CM12	17	2.03	-1.98		CM12	13	2.05	-1.93
CM12	8	2.08	-1.88		CM12	21	2.00	-1.99
CM12	28	2.01	-1.94		CM12	20	2.05	-1.91
CM12	38	2.03	-1.92		CM12	23	2.09	-1.93
CM12	35	2.13	-1.82		CM12	22	1.84	-2.31
CM12	15	1.94	-2.11		CM12	9	1.86	-2.15
CM12	27	1.99	-1.98		CM12	18	1.94	-2.13
CM12	15	2.10	-1.91		CM12	31	2.10	-1.82
CM12	39	2.07	-1.84		CM12	23	2.06	-1.95
CM12	44	2.05	-1.88		CM12	43	2.04	-1.91
CM12	41	2.04	-1.90		CM12	26	2.00	-1.96
CM12	47	2.06	-1.94		CM12	43	2.07	-1.96
CM12	58	2.03	-1.99		CM12	33	2.05	-1.87
CM12	33	2.22	-1.58		CM12	41	2.07	-1.87
CM12	32	2.11	-1.82		CM12	29	2.03	-1.92
CM12	34	1.86	-2.17		CM12	39	2.08	-1.89
CM12	37	2.16	-1.69		CM12	56	2.03	-1.91
CM12	34	2.09	-1.87		CM12	26	2.02	-1.95

Table 15

Standard	Weight (ug)	d13C	d18O		Standard	Weight (ug)	d13C	d18O
NBS18	38	-5.05	-22.99		NBS18	68	-5.04	-23.07
NBS18	28	-5.07	-23.03		NBS18	35	-5.03	-23.09
NBS18	15	-4.97	-23.04		NBS18	27	-5.00	-22.99
NBS18	14	-5.02	-23.06		NBS18	23	-5.00	-22.95
NBS18	22	-5.04	-22.99		NBS18	26	-5.03	-23.04
NBS18	20	-4.88	-23.08		NBS18	26	-5.01	-22.97
NBS18	44	-5.03	-22.89		NBS18	7	-4.96	-22.97
NBS18	22	-5.03	-23.02		NBS18	68	-5.04	-23.07
NBS18	27	-5.09	-23.02		NBS18	52	-5.05	-22.95
NBS18	32	-4.92	-22.99		NBS18	34	-5.03	-23.09
NBS18	38	-5.17	-23.35		NBS18	22	-5.00	-22.98
NBS18	77	-4.81	-22.63		NBS18	39	-4.95	-23.02
NBS18	151	-5.18	-23.42		NBS18	18	-5.06	-22.93
NBS18	89	-4.88	-22.64		NBS18	23	-5.10	-23.13
NBS18	26	-5.03	-23.04		NBS18	33	-5.02	-23.06
NBS18	26	-5.01	-22.97		NBS18	9	-4.85	-22.92
NBS18	7	-4.96	-22.97					

Table 16

Standard	Weight (ug)	d13C	d18O
Atlantis II	19	1.01	3.43
Atlantis II	12	0.97	3.30
Atlantis II	23	0.93	3.35
Atlantis II	24	0.73	2.98
Atlantis II	30	1.08	3.75
Atlantis II	28	0.86	3.04
Atlantis II	15	0.68	2.95
Atlantis II	20	0.94	3.45
Atlantis II	30	0.88	3.34
Atlantis II	28	0.86	3.04
Atlantis II	15	0.68	2.95
Atlantis II	87	0.81	3.33
Atlantis II	45	0.87	3.45
Atlantis II	34	0.92	3.26
Atlantis II	32	0.80	3.25
Atlantis II	53	0.71	3.41
Atlantis II	18	0.85	3.45
Atlantis II	10	1.06	3.58
Atlantis II	22	0.81	3.37

Table 17

Data Table Captions

Table 1: Stable isotopic data for *Acarinina* spp. from SDB. Delta values expressed relative to vPDB.

Table 2: Stable isotopic data for *Morozovella* spp. from SDB. Delta values expressed relative to vPDB.

Table 3: Stable isotopic data for *Subbotina* spp. from SDB. Delta values expressed relative to vPDB.

Table 4: Corrected stable isotopic data for benthic foraminifera from SDB. Delta values expressed relative to vPDB. Affected data marked with an asterisk (*).

Table 5: Stable isotopic data for selected benthic foraminifera from SDB as well as duplicated measurements used in the correction process. Offsets are also calculated in the far-right columns. Delta values expressed relative to vPDB.

Table 6: Uncorrected stable isotopic data for benthic foraminifera from SDB from the affected interval. Delta values expressed relative to vPDB.

Table 7: Mg/Ca data for all planktonic foraminifera from SDB. Mg/Ca values are in mmol/mol.

Table 8: Mg/Ca data for all benthic foraminifera from SDB.

Table 9: Stable isotopic data for *Acarinina* spp. from Cam-Dor. Delta values expressed relative to vPDB.

Table 10: Stable isotopic data for *Morozovella* spp. from Cam-Dor. Delta values expressed relative to vPDB.

Table 11: Stable isotopic data for *Subbotina* spp. from Cam-Dor. Delta values expressed relative to vPDB.

Table 12: Stable isotopic data for all benthic foraminifera from Cam-Dor. Delta values expressed relative to vPDB.

Table 13: Mg/Ca data for all planktonic foraminifera from Cam-Dor. Mg/Ca values are in mmol/mol.

Table 14: Mg/Ca data for all benthic foraminifera from Cam-Dor. Mg/Ca values are in mmol/mol.

Table 15: Stable isotopic values for all Carrera Marble (CM12) standards used in this study. Delta values expressed relative to vPDB.

Table 16: Stable isotopic values for all NBS 18 standards used in this study. Delta values expressed relative to vPDB.

Table 17: Stable isotopic values for all Atlantis II standards used in this study. Delta values expressed relative to vPDB.

Appendix

SDB Benthic C and O Isotope Data Corrections:

For SDB, one run (8/18/17) of benthic $\delta^{13}C$ and $\delta^{18}O$ as marked by asterisks (Tables 4-6) were corrected for a line offset bias in the Kiel/Mat253 mass spectrometer through the depth interval from 202.1 -187.2 m. Line 1 was noticeably depleted relative to line 2 displaying a covariance between isotopic values derived from each line on the carbon and oxygen curves. This was corrected for by running three duplicate samples for samples run through line 1 and 4 duplicate samples for samples run through line two. The difference between each isotopic value and its duplicate was calculated and each line's offsets were averaged. The line 1 offset average was added to uncorrected carbon and oxygen values to achieve corrected values. The line 2 offset average was subtracted from uncorrected carbon and oxygen values to achieve corrected isotope values through the affected interval. As a consequence, the error on these values is ±0.2‰.

Oxygen Isotope Estimated Temperature

$\delta^{18}O$ derived temperature estimates for both planktonic and benthic foraminifera were done using oxygen temperature calibrations from (Bemis et al., 1998; Marchitto et al., 2014). Three equations have been derived based on depth habitat and ecology (symbiont vs. non-symbiont). Equation 1 for low

light cultures describes the relationship between seawater temperature and the difference between $\delta^{18}O$ of foraminifera calcite and $\delta^{18}O$ of seawater. This relationship is linear and is described by the equation:

$$T(℃) = 16.5(\pm 0.2) - 4.80(\pm 0.16) * (\delta_c - \delta_w) \quad (1)$$

where δ_c is $\delta^{18}O$ (vPDB) of calcite and δ_w is $\delta^{18}O$ (vPDB: after conversion from vSMOW) of the seawater in which if formed. This equation was used for temperature estimates for symbiotic planktonic foraminifera *Acarinina* spp. and *Morozovella* spp. Equation 2 for 11 chambered shell foraminifera describes the relationship between seawater temperature and the difference between $\delta^{18}O$ (vPDB) of foraminifera calcite and $\delta^{18}O$ (vPDB: after conversion from vSMOW) of seawater. This relationship is also linear and is described by the equation:

$$T(℃) = 12.6(\pm 0.3) - 5.07(\pm 0.22) * (\delta_c - \delta_w) \quad (2)$$

This equation was used for temperature estimates for asymbiotic planktonic foraminifera *Subbotina* spp. For benthic oxygen temperature estimation, Marchitto et al. 2014 was used. The relationship between temperature and the difference between $\delta^{18}O$ of foraminifera calcite and $\delta^{18}O$ of seawater is described by equation 3:

$$t = \frac{0.245\sqrt{0.045461 + 0.0044(\delta_{cp} - \delta_{ws})}}{0.0022} \quad (3)$$

where δ_{cp} is the $\delta^{18}O$ (vPDB) of calcite and δ_{ws} is the $\delta^{18}O$ (vPDB: after conversion from vSMOW) of the seawater in which if formed. This equation is calibrated for modern benthic foraminifera *Cibicidoides* spp.

Because these equations describe the relationship between $\delta^{18}O$ of foraminifera calcite and $\delta^{18}O$ of seawater, an estimate for Paleocene/Eocene $\delta^{18}O$ of seawater is necessary. Based on modern observations Zachos et al. (1994) developed a simple expression to represent changes in latitudinal zonal averages of $\delta^{18}O$ seawater gradients with quadratic equation 4:

$$y = 0.576 + 0.041x = 0.0017x^2 + 0.0000135x^3 \qquad (4)$$

where y is the local seawater and x is the absolute latitude. Simply plugging in the paleo-latitude for the mid-Atlantic shelf sites (~39°N) produces an estimate for local $\delta^{18}O$ of seawater in vSMOW. The Bemis et al., (1998) equations require $\delta^{18}O$ values in vPDB. Therefore, the conversion used is equation 5:

$$\delta 18\mathrm{Osw\ (vPDB)} = \delta 18\mathrm{Osw\ (vSMOW)} - 2.7‰ \qquad (5)$$

Mg/Ca Estimate Temperature

Mg/Ca temperature determination for all planktonic foraminifera analyzed in this study was done using (Evans et al. 2012). Temperature calibrations produced the exponential equation:

$$Mg/Ca_{test} = \frac{F\ x\ Mg/Ca_{sw}^{t=t^H}}{F\ x\ Mg/Ca_{sw}^{t=0^H}} * Bexp^{AT} \quad (6)$$

Species specific exponential constants F, H, B and A are 2.5, 0.41, 0.38 and 0.09. F and H were taken from calibration study (Delaney et al. 1985) and B and A were taken from multi-species calibration study (Anand et al. 2003). A crucial part of this Mg/Ca temperature calibration is an accurate estimate of Paleocene/Eocene Mg/Ca_{sw}. Mg/Ca in seawater has varied through time, however, it residence time is long enough to assume it is unchanging through a relatively short-lived event such as the PETM. For this study, a range of paleo-Mg/Ca_{sw} was considered from 2.0-3.0 mmol/mol (Evans et al., 2016) as well as a modern Mg/Ca_{sw} of 5.2 mmol/mol (Lowenstein et al., 2001).

Because existing Mg/Ca based temperature calibration studies of benthic foraminifera are based on pelagic genera, the temperature estimations for the shallow marine taxa studied here likely have a large error. A series of calibrations were considered including (Lear et al., 2002; Elderfield et al., 2006; Marchitto et al., 2007 and Bryan et al., 2008). Due to its closer agreement with oxygen isotope derived temperatures, Marchitto et al., (2007) was considered the most appropriate. This calibration study used modern *Cibicidoides* spp. taken from the Florida Strait to produce equation 7:

$$Mg/Ca = 1.55 \pm 0.12e^{0.042 \pm 0.005T} \quad (7)$$

Salinity Estimate Procedure

Sea surface salinity estimates were done in accordance with Zachos et al., (2003) where coupled oxygen and Mg/Ca temperatures were used to quantify salinity during the PETM. The process involves first calculating C values with equation 8:

$$C = \left[\left(\frac{y_2}{y_1} - 1\right)100\right] \quad (8)$$

The C value is the percent change in Mg/Ca (y_2) relative to some baseline Mg/Ca value (y_1). The baseline value was chosen with the assumption that it represents a normal pre-CIE Mg/Ca ratio. Using the C values, ΔT was calculated at each depth interval using equation 9:

$$\Delta T = \frac{1}{m} ln\left[\left(\frac{C}{100}\right) + 1\right] \quad (9)$$

ΔT is a calculated change in temperature relative to the previously set baseline Mg/Ca value. Variable m is an assumed temperature sensitivity based off of previously constrained exponential constants for planktonic foraminifera (A=0.9) (Anand et al. 2003). ΔT was then converted to relative changes in $\delta^{18}O$ based off of known $\delta^{18}O$/temperature sensitivities (Zachos et al. 2003). Measured $\delta^{18}O$ values and theoretical Mg/Ca derived $\delta^{18}O$ values were subtracted and the difference represents the $\delta^{18}O$ anomaly or the salinity contribution to measured $\delta^{18}O$. Conversion of the $\delta^{18}O$ anomaly to relative changes in salinity was achieved with the Zachos et al., (2003) salinity conversion range of 0.25 to 0.5 per p.s.u.

Testing Mg/Ca and Oxygen Temperature Sensitivities

Because Mg/Ca temperatures calibrations as a whole are not as well constrained as oxygen isotope derived temperatures, it is assumed that oxygen isotope derived temperatures are closer to the true absolute temperatures. For this exercise, the Mg/Ca data generated from SDB and Cam-Dor are in a sense calibrated against the oxygen isotope derived temperatures from the same specimens. One assumption that must be made is that the local $\delta^{18}O$ of seawater is not changing as that would obviously effect oxygen derived temperatures and not the Mg/Ca data, thus skewing the relationship. This however, is not the case as the local $\delta^{18}O$ of seawater must be changing in an event that is associated with major surface water freshening. Yet, this exercise can be an important way to constrain Mg/Ca derived temperatures.

In the main text, regressions (Figures 15 and 16) are used to determine the sensitivity of benthic Mg/Ca data against $\delta^{18}O$ derived temperatures for sites South Dover Bridge and Cambridge-Dorchester. In Figure 15, linear regressions were used to fit data and generate respective calibration equations. In figure 16, exponential regressions were used to fit data and generate respective calibration equations. R-squared values (R^2) measure the strength of the Mg/Ca data and oxygen temperature relationship. Exponential regression models generally display better results than linear

regression models. Planktonic foraminifera yield more robust regressions with R-squared values ranging from 0.53 to 0.87 for both linear and exponential fits. Given the limited range of temperatures (<3 to 5°C) recorded with individual species across the PETM, this relationship is only weakly constrained with the benthic taxa in this study with the exception of *A. acutus* from SDB which has R^2 values of 0.76 and 0.83 for linear and exponential models respectively. *Cibicidoides* spp. from SDB and Cam-Dor as well as *A. acutus* from Cam-Dor all display low correlation with R^2 values under 0.15.

References

Anand, P., Elderfield, H., and Conte, M. H., 2003, Calibration of Mg/Ca thermometry in planktonic foraminifera from a sediment trap time series: Paleoceanography, v. 18, no. 2, p. 15.

Babila, T. L., Rosenthal, Y., Wright, J. D., and Miller, K. G., 2016, A continental shelf perspective of ocean acidification and temperature evolution during the Paleocene-Eocene Thermal Maximum: Geology, v. 44, no. 4, p. 275-278.

Barker, S., Greaves, M., and Elderfield, H., 2003, A study of cleaning procedures used for foraminiferal Mg/Ca paleothermometry: Geochemistry Geophysics Geosystems, v. 4, p. 20.

Bemis, B. E., Spero, H. J., Bijma, J., and Lea, D. W., 1998, Reevaluation of the oxygen isotopic composition of planktonic foraminifera: Experimental results and revised paleotemperature equations: Paleoceanography, v. 13, no. 2, p. 150-160.

Bijma, J., Faber, W. W., and Hemleben, C., 1990, TEMPERATURE AND SALINITY LIMITS FOR GROWTH AND SURVIVAL OF SOME PLANKTONIC FORAMINIFERS IN LABORATORY CULTURES: Journal of Foraminiferal Research, v. 20, no. 2, p. 95-116.

Bowen, G. J., Maibauer, B. J., Kraus, M. J., Rohl, U., Westerhold, T., Steimke, A., Gingerich, P. D., Wing, S. L., Clyde, W. C., 2014, Two

massive, rapid releases of carbonduring the onset of the Palaeocene-Eocene thermal maximum, GEOLOGY& GEOPHYSICS, V. 8, no. 1, p. 44-47.

Boyle, E. A., and Keigwin, L. D., 1985, COMPARISON OF ATLANTIC AND PACIFIC PALEOCHEMICAL RECORDS FOR THE LAST 215,000 YEARS - CHANGES IN DEEP OCEAN CIRCULATION AND CHEMICAL INVENTORIES: Earth and Planetary Science Letters, v. 76, no. 1-2, p. 135-150.

Bryan, S. P., and Marchitto, T. M., 2008, Mg/Ca-temperature proxy in benthic foraminifera: New calibrations from the Florida Straits and a hypothesis regarding Mg/Li: Paleoceanography, v. 23, no. 2, p. 17.

Dhondt, S., Zachos, J. C., and Schultz, G., 1994, STABLE ISOTOPIC SIGNALS AND PHOTOSYMBIOSIS IN LATE PALEOCENE PLANKTIC FORAMINIFERA: Paleobiology, v. 20, no. 3, p. 391-406.

Elderfield, H., Yu, J., Anand, P., Kiefer, T., and Nyland, B., 2006, Calibrations for benthic foraminiferal Mg/Ca paleothermometry and the carbonate ion hypothesis: Earth and Planetary Science Letters, v. 250, no. 3-4, p. 633-649.

Evans, D., and Müller, W., 2012, Deep time foraminifera Mg/Ca paleothermometry: Nonlinear correction for secular change in seawater Mg/Ca: Paleoceanography, v. 27, p. 11.

Evans, D., Wade, B. S., Henehan, M., Erez, J., and Muller, W., 2016, Revisiting carbonate chemistry controls on planktic foraminifera Mg/Ca: implications for sea surface temperature and hydrology shifts over the Paleocene Eocene Thermal Maximum and Eocene Oligocene transition: Climate of the Past, v. 12, no. 4, p. 819-835.

Gibson, T. G., Bybell, L. M., and Mason, D. B., 2000, Stratigraphic and climatic implications of clay mineral changes around the Paleocene/Eocene boundary of the northeastern US margin: Sedimentary Geology, v. 134, no. 1-2, p. 65-92.

John, C. M., Bohaty, S. M., Zachos, J. C., Sluijs, A., Gibbs, S., Brinkhuis, H., and Bralower, T. J., 2008, North American continental margin records of the Paleocene-Eocene thermal maximum: Implications for global carbon and hydrological cycling: Paleoceanography, v. 23, no. 2, p. 20.

Kelly, D. C., Bralower, T. J., Zachos, J. C., Premoli Silva, I., and Thomas, E., Rapid diversification of planktonic foraminifera in the tropical Pacific (ODP Site 865) during the late Paleocene thermal maximum, *Geology*, 24, 423-426, 1996.

Kennett, J. P., and Stott, L. D., 1991, ABRUPT DEEP-SEA WARMING, PALAEOCEANOGRAPHIC CHANGES AND BENTHIC EXTINCTIONS AT THE END OF THE PALEOCENE: Nature, v. 353, no. 6341, p. 225-229.

Koch, P. L., Zachos, J. C., and Gingerich, P. D., 1992, CORRELATION BETWEEN ISOTOPE RECORDS IN MARINE AND CONTINENTAL CARBON RESERVOIRS NEAR THE PALEOCENE EOCENE BOUNDARY: Nature, v. 358, no. 6384, p. 319-322.

Kopp, R. E., Schumann, D., Raub, T. D., Powars, D. S., Godfrey, L. V., Swanson-Hysell, N. L., Maloof, A. C., and Vali, H., 2009, An Appalachian Amazon? Magnetofossil evidence for the development of a tropical river-like system in the mid-Atlantic United States during the Paleocene-Eocene thermal maximum: Paleoceanography, v. 24, p. 17.

Lear, C. H., Rosenthal, Y., and Slowey, N., 2002, Benthic foraminiferal Mg/Ca-paleothermometry: A revised core-top calibration: Geochimica Et Cosmochimica Acta, v. 66, no. 19, p. 3375-3387.

Lippert, P. C., and Zachos, J. C., 2007, A biogenic origin for anomalous fine-grained magnetic material at the Paleocene-Eocene boundary at Wilson Lake, New Jersey: Paleoceanography, v. 22, no. 4, p. 8.

Lowenstein, T. K., Timofeeff, M. N., Brennan, S. T., Hardie, L. A., and Demicco, R. V., 2001, Oscillations in Phanerozoic seawater chemistry: Evidence from fluid inclusions: Science, v. 294, no. 5544, p. 1086-1088.

Luciani, V., D'Onofrio, R., Dickens, G. R., and Wade, B. S., 2017, Planktic foraminiferal response to early Eocene carbon cycle perturbations in

the southeast Atlantic Ocean (ODP Site 1263): Global and Planetary Change, v. 158, p. 119-133.

Makarova, M., Wright, J. D., Miller, K. G., Babila, T. L., Rosenthal, Y., and Park, J. I., 2017, Hydrographic and ecologic implications of foraminiferal stable isotopic response across the US mid-Atlantic continental shelf during the Paleocene-Eocene Thermal Maximum: Paleoceanography, v. 32, no. 1, p. 56-73.

Marchitto, T. M., Bryan, S. P., Curry, W. B., and McCorkle, D. C., 2007, Mg/Ca temperature calibration for the benthic foraminifer Cibicidoides pachyderma: Paleoceanography, v. 22, no. 1, p. 9.

Marchitto, T. M., Curry, W. B., Lynch-Stieglitz, J., Bryan, S. P., Cobb, K. M., and Lund, D. C., 2014, Improved oxygen isotope temperature calibrations for cosmopolitan benthic foraminifera: Geochimica Et Cosmochimica Acta, v. 130, p. 1-11.

McInerney, F. A., and Wing, S. L., 2011, The Paleocene-Eocene Thermal Maximum: A Perturbation of Carbon Cycle, Climate, and Biosphere with Implications for the Future: Annual Review of Earth and Planetary Sciences, Vol 39, v. 39, p. 489-516.

Pagani, M., Pedentchouk, N., Huber, M., Sluijs, A., Schouten, S., Brinkhuis, H., Damste, J. S. S., Dickens, G. R., and Expedit, S., 2006, Arctic hydrology during global warming at the Palaeocene/Eocene thermal maximum: Nature, v. 442, no. 7103, p. 671-675.

Pearson, P., Olsson, R. K., Huber, B., Coxall, H. K., 2006, Atlas of Eocene Planktonic Foraminifera: Overview of Eocene planktonic foraminifera taxonomy, paleoecology, phylogeny, and biostratigraphy, Cushman Foundation Special Publication.

Penman, D. E., Honisch, B., Zeebe, R. E., Thomas, E., and Zachos, J. C., 2014, Rapid and sustained surface ocean acidification during the Paleocene-Eocene Thermal Maximum: Paleoceanography, v. 29, no. 5, p. 357-369.

Rohl, U., Westerhold, T., Bralower, T. J., and Zachos, J. C., 2007, On the duration of the Paleocene-Eocene thermal maximum (PETM): Geochemistry Geophysics Geosystems, v. 8.

Self-Trail, J. M., Powars, D. S., Watkins, D. K., and Wandless, G. A., 2012, Calcareous nannofossil assemblage changes across the Paleocene-Eocene Thermal Maximum: Evidence from a shelf setting: Marine Micropaleontology, v. 92-93, p. 61-80.

Self-Trail, J. M., Robinson, M. M., Bralower, T. J., Sessa, J. A., Hajek, E. A., Kump, L. R., Trampush, S. M., Willard, D. A., Edwards, L. E., Powars, D. S., and Wandless, G. A., 2017, Shallow marine response to global climate change during the Paleocene-Eocene Thermal Maximum, Salisbury Embayment, USA: Paleoceanography, v. 32, no. 7, p. 710-728.

Sluijs, A., and Brinkhuis, H., 2009, A dynamic climate and ecosystem state during the Paleocene-Eocene Thermal Maximum: inferences from dinoflagellate cyst assemblages on the New Jersey Shelf: Biogeosciences, v. 6, no. 8, p. 1755-1781.

Stassen, P., Thomas, E., and Speijer, R. P., 2012, Integrated stratigraphy of the Paleocene-Eocene thermal maximum in the New Jersey Coastal Plain: Toward understanding the effects of global warming in a shelf environment: Paleoceanography, v. 27, p. 17.

Stassen, P., 2015, Paleocene-Eocene Thermal Maximum environmental change in the New Jersey Coastal Plain: benthic foraminiferal biotic events: Marine Micropaleontology, v. 115, p. 1-23.

Tripati, A. K., and Elderfield, H., 2004, Abrupt hydrographic changes in the equatorial Pacific and subtropical Atlantic from foraminiferal Mg/Ca indicate greenhouse origin for the thermal maximum at the Paleocene-Eocene Boundary: Geochemistry Geophysics Geosystems, v. 5.

Tripati, A. K., and Elderfield, H., 2005, Deep-sea temperature and circulation changes at the Paleocene-Eocene thermal maximum: Science, v. 308, no. 5730, p. 1894-1898.

Wright, J. D., and Schaller, M. F., 2013, Evidence for a rapid release of carbon at the Paleocene-Eocene thermal maximum: Proceedings of the National Academy of Sciences of the United States of America, v. 110, no. 40, p. 15908-15913.

Zachos, J. C., Stott, L. D., and Lohmann, K. C., 1994, EVOLUTION OF EARLY CENOZOIC MARINE TEMPERATURES: Paleoceanography, v. 9, no. 2, p. 353-387.

Zachos, J. C., Wara, M. W., Bohaty, S., Delaney, M. L., Petrizzo, M. R., Brill, A., Bralower, T. J., and Premoli-Silva, I., 2003, A transient rise in tropical sea surface temperature during the Paleocene-Eocene Thermal Maximum: Science, v. 302, no. 5650, p. 1551-1554.

Zachos, J. C., Rohl, U., Schellenberg, S. A., Sluijs, A., Hodell, D. A., Kelly, D. C., Thomas, E., Nicolo, M., Raffi, I., Lourens, L. J., McCarren, H., and Kroon, D., 2005, Rapid acidification of the ocean during the Paleocene-Eocene thermal maximum: Science, v. 308, no. 5728, p. 1611-1615.

Zachos, J. C., Schouten, S., Bohaty, S., Quattlebaum, T., Sluijs, A., Brinkhuis, H., Gibbs, S. J., and Bralower, T. J., 2006, Extreme warming of mid-latitude coastal ocean during the Paleocene-Eocene Thermal Maximum: Inferences from TEX86 and isotope data: Geology, v. 34, no. 9, p. 737-740.

Zachos, J. C., Stott, L. D., and Lohmann, K. C., 1994, EVOLUTION OF EARLY CENOZOIC MARINE TEMPERATURES: Paleoceanography, v. 9, no. 2, p. 353-387.

Zachos, J. C., Wara, M. W., Bohaty, S., Delaney, M. L., Petrizzo, M. R., Brill, A., Bralower, T. J., and Premoli-Silva, I., 2003, A transient rise in

tropical sea surface temperature during the Paleocene-Eocene Thermal Maximum: Science, v. 302, no. 5650, p. 1551-1554.